Dancing sprites: detailed analysis of two case studies

Serge Soula[1], Janusz Mlynarczyk[2], Martin Füllekrug[3], Nicolau Pineda[4], Jean-François Georgis[1], Oscar van der Velde[5], Joan Montanyà[5], Ferran Fabro[5]

1. University of Toulouse/CNRS, Laboratory of Aerology, 14 avenue Edouard Belin, 31400 Toulouse, France.
2. Department of Electronics, AGH University of Science and Technology, Krakow, Poland
3. University of Bath, Department of Electronic and Electrical Engineering, Bath, United Kingdom.
4. Remote Sensing Unit, Meteorological Service of Catalonia, c/Berlín 38-46, E-08029 Barcelona, Spain.
5. Electrical Engineering Department, Technological University of Catalonia, Terrassa, Spain

Abstract. During the night of October 29-30, 2013, a low-light video camera installed at Pic du Midi (2877 m) in the Pyrénées, recorded TLEs above a very active storm over the Mediterranean Sea. The minimum cloud top temperature reached -73°C at ~1600 UTC while its cloud to ground (CG) flash rate exceeded 30 fl min^{-1}. Some sprite events have long duration ~~last one second or more~~ and resemble to dancing sprites. We analyze in detail the temporal evolution and estimated location of sprite elements for two series of sprite sequences, ~~of them~~ as well as the cloud structure, the lightning activity, the electric field radiated in a broad range of low frequencies and the current moment waveform of the lightning strokes. (i) In each series, ~~event~~ successive sprite ~~elements~~ sequences reflect the occurrence time and location of individual positive lightning strokes across the stratiform region. (ii) The longer time-delayed (> 20 ms) sprite elements correspond to the lower impulsive charge moment changes (iCMC) of the parent stroke (< 200 C km) and they are shifted few tens of kilometres from their SP+CG stroke. However, both short and long time-delayed sprite elements also occur after strokes that produce a large iCMC and that are followed by a continuing current. (iii) The long time-delayed sprite elements produced during the continuing current correspond to surges in the current moment waveform. They occur sometimes at an altitude apparently lower than the previous short time-delayed sprite elements, possibly because of the lowered altitude of the ionosphere potential. (iv) The largest and

brightest sprite elements produce significant current signatures, visible when their delay is not too short (~3-5 ms).

1. Introduction

Sprites are luminous discharges observed above thunderstorms and they are classified as one specific type of transient luminous events (TLE) since the beginning of 1990s when they were incidentally discovered (*Franz et al.*, 1990). Thereafter, observational campaigns in the US provided a wealth of information to understand the underlying physical processes [*Sentman and Wescott*, 1993; *Lyons*, 1996; *Sentman et al.*, 1995]. The turn of the millenium marked the observation of sprites almost anywhere in the world [*Vaughan et al.*, 1992; *Boeck et al.*, 1995; *Fukunishi et al.* 1999; *Neubert et al.*, 2001; *Su et al.* 2002; *Pinto et al.*, 2004; *Yang et al.*, 2008, *Chen et al.*, 2008].

Sprite discharges span over an altitude range from ~40-90 km [*Sentman and Wescott*, 1993; *McHarg et al.*, 2002; *Soula et al.*, 2014] and they have various shapes that classifies sprites in several types, e.g., columnar, carrot, jellyfish, angel, [*Lyons et al.*, 2003; *Williams*, 2001; *Neubert et al.*, 2008; *Bór*, 2013]. Telescopic imaging revealed that sprites have a fine structure of streamers [*Gerken et al.*, 2000], and high-speed camera recordings showed the development of complex forms in detail [*Stanley et al.*, 1999; *Moudry et al.*, 2003; *McHarg et al.*, 2007; *Stenbaek-Nielsen and McHarg*, 2008; *Li and Cummer*, 2009; *Montanyà et al.*, 2010; *Stenbaek-Nielsen et al.*, 2010]. Sprites can also horizontally extend over several tens of km in the form of sprite clusters [*Sentman et al.*, 1995; *Füllekrug et al.*, 2001, *Soula et al.*, 2014] and they can even occur over more than ~100 km in the form of sequential luminous emissions that are called dancing or jumping sprites [*Winckler et al.*, 1996; *Lyons*, 1996; *Füllekrug et al.*, 2013a, *Lu et al.*, 2013; *Yang et al.*, 2015]. These sprite elements that seem to "dance" above a large area of the storm, are still enigmatic according to *Lu et al.* (2013). These authors observed ~~that the~~ several cases of dancing sprites ~~are~~ associated with a single lightning flash and noted the dancing sprites could have been produced ~~either~~ by distinct strokes of the flash, by a single stroke through a series of current surges superposed on an intense continuing current, or by both.

Most of the time, sprites occur above stratiform regions of Mesoscale Convective Systems (MCS), shortly after parent positive cloud-to-ground (SP+CG) strokes that lower a large amount of charge to the ground [*Boccippio et al.*, 1995; *Lyons*, 1996; *São Sabbas et al.*, 2003; 2010;

63 *Cummer and Lyons*, 2005; *Soula et al.*, 2009]. The rate of sprite production can reach several
64 hundreds of events for a unique storm activity when the size and the duration of the storm system
65 are large [*Lyons*, 1994; *São Sabbas et al.*, 2010]. The necessary condition for a storm to produce
66 large rates of sprites is a strong charge generation, possibly related to the convective vigour but
67 also to favourable conditions of charge generation due to large concentrations of aerosol particles
68 within the troposphere as suggested by *Lyons et al.* [1998] and *São Sabbas et al.* [2010].
69 After the SP+CG stroke, the sprite discharge develops as a streamer, a result of the strong
70 transient electrostatic field that exceeds the threshold for dielectric breakdown in the middle
71 atmosphere, generally around 70 km [*Pasko et al.*, 1997]. The time delay between the SP+CG
72 stroke and the sprite ranges from a few milliseconds to several tens of milliseconds [*Bell et al.*,
73 1998; *Cummer and Lyons*, 2005; *van der Velde et al.*, 2006]. It depends on the characteristics of
74 the SP+CG stroke, especially in terms of charge moment change (CMC), impulsive CMC
75 (iCMC) and current waveforms [*Soula et al.*, 2015]. It can reach a few tens of ms after a long
76 lightning continuing current following the stroke [*Cummer and Füllekrug*, 2001]. Thanks to a
77 triangulation of several sprites and a three-dimensional mapping of the parent lightning flashes,
78 *Lu et al.* [2013] showed that short time delayed sprites (< 20 ms) were less horizontally displaced
79 (typically <30 km) from the ground stroke than long time delayed sprites. They showed also that
80 for any time delay the sprite elements were in good spatial correspondence with negative stepped
81 leaders detected during the prior 100 ms interval.
82 Most of the SP+CG flashes start close to the convective cores of the storm and horizontally
83 extend into stratiform region that consists of several layers of alternating charge polarity at
84 different altitudes. These flashes are supposed to follow trajectories of charged ice particles
85 rearward of the storm system [*Carey et al.*, 2005; *Ely et al.*, 2008; *van der Velde et al.*, 2010;
86 2014]. Some of these flashes can be considered as spider lightning [*Mazur et al.*, 1998; *Lang et*
87 *al.*, 2004]. According to *Mazur et al.* [1998] the spider lightning flashes occur in the stratiform
88 region of decaying storms and produce negative leaders propagating over several tens of
89 kilometres with a speed of 2-4 10^5 m s^{-1}. They also noted that the interferometer they used could
90 not map this kind of negative leader because several branches develop simultaneously. The
91 spider lightning flashes can have several attachments to the ground, with positive and negative
92 polarity, along their horizontal extent [*Lang et al.*, 2004; *Soula et al.*, 2010]. In a recent work,
93 *van der Velde* et al. [2014] analysed the bidirectional development of several flashes associated

with sprite production. They identified different modes of propagation of the negative leaders throughout the thundercloud that are associated with different location and timing of the positive +CG strokes. Thus, the negative leaders may propagate at various altitudes with different velocities and over various distances, while generating several multiple +CG strokes. However, SP+CG flashes can also initiate in small convective cells, where they generally occur in the decaying convective region [*van der Velde et al.*, 2010].

This study investigates a long lifetime storm that produced a large number of sprites, including dancing sprites ~~In particular, two sprite events are analyzed in detail because they seem to be dancing sprites,~~ that are not well characterized and studied in the scientific literature. Section 2 describes the data used in the study, section 3 provides the characteristics of the thunderstorm and section 4 describes the ~~sequences~~ conditions of sprite production ~~emissions~~ at the scale of the storm and in detail for two series of dancing sprites. Section 5 discusses the results and section 6 summarizes the main findings in the conclusions.

2. Data

2.1. Optical observations

The videos used in this study are recorded with a camera installed at Pic du Midi (42.93N; 0.14E; 2877 m), as indicated in Figure 1. This camera can be oriented to the storm with a pan-tilt unit that can be remotely controlled via the Internet. The camera is a low-light Watec 902H (minimum illumination of 0.0001 lux) with a field of view (FOV) of 31° and a high-resolution charge-coupled device (CCD). It operates in a triggered mode provided by the UFOCaptureV2 software (http://sonotaco.com/soft/e_index.html#ufocv2, accessed date) to capture luminous events with brightness above a given threshold. The video imagery obtained has a time resolution of 25 frames (or 50 interlaced fields) per second, which corresponds to a time resolution of 20 milliseconds. The images of the videos are de-interlaced for the analysis. The video camera also records GPS-referenced time and inserts the time in each video frame. Table 1 displays the terms we use in the paper in order to specify the sprite activity at different scales of time. Event specifies sprite occurrence at the scale of a video that lasts 1 or 2 seconds. Some videos included several groups of sprite elements, thus we use sequence for successive sprite fields following a same lightning stroke (as in *Lu et al.* [2013]) and series for a group of

sequences that are included in the same video and that are associated to successive strokes that belong (or not) to the same flash.

The azimuth and elevation of the sprite events are determined with the software "Cartes du Ciel" (SkyCharts) as described in *van der Velde* [2008]. The principle of the software is to overlay known stars on an image from the video imagery, stating the date, time and place of observation. The matching of the stars with those in the image is manually done and empirically. This method usually works very well when enough stars are visible. For a sprite event, the azimuths can be determined for each individual element that constitutes the sprite event. A sprite is usually much wider than the read-out of the azimuth, which varies typically only within ~0.17°. The altitude is estimated by using the elevation and the great circle distance, assuming that the distance of the sprite is the same distance between the SP+CG stroke and the video camera. Thus, the vertical scale in the fields is determined for each sequence of sprite elements that corresponds to a SP+CG stroke. This method introduces an error estimated for example between 7 and 8 km when the distance of the sprite from the camera is around 400 km and the error on it of 40 km. The value of 40 km for the displacement of the sprite is the average found by *Sao Sabbas et al.* [2003]. For short time delayed sprites (< 20 ms), this displacement is usually lower than 30 km according to *Lu et al.* [2013].

The delay Δt can be only determined as a value interval:

$$\Delta t \in [0 ; t_e - t_s] \text{ when } t_e > t_s > t_b$$

$$\Delta t \in [t_b - t_s ; t_e - t_s] \text{ when } t_b > t_s$$

t_b, t_e, and t_s are the times of the beginning and the end of the first field with sprite luminosity and the time of the stroke, respectively.

2.2. Lightning detection

Several location systems monitor the lightning flash activity within the studied area during the period of the storm analyzed. First, the European lightning detection network operated by European Cooperation for Lightning Detection (EUCLID) records CG flash characteristics such as the location, polarity, peak current, and the occurrence times of CG strokes [*Soula et al.*, 2010; *Poelman et al.*, 2016]. The sensors of the network use both magnetic direction finding (MDF) and time of arrival (TOA) techniques to determine the location of CG strokes [*Cummins*

154 *and Murphy*, 2009]. EUCLID data allows us to identify lightning flashes with a temporal and
155 spatial resolution of ~0.5 s and ~10 km [*Cummins et al.*, 1998]. However, in this study, both
156 individual strokes and CG flashes can be used, according to the requirements of the study. The
157 detection efficiency (DE) of this network is ~90% over land and close to the coastline, but in the
158 present study and according to the storm location over the Mediterranean, the DE can be lower
159 than 90%.

160 Second, the Lightning Mapping System XDDE operated by the Meteorological Service of
161 Catalonia (SMC) allows monitoring total lightning (IC + CG) activity in Catalonia (northeastern
162 Spain) [*Pineda and Montanyà*, 2009]. This system is composed of four VAISALA LS8000 and
163 one TLS200 interferometric stations that operate as a very high frequency (VHF) interferometer
164 from ~110-118 MHz. Each station determines azimuthal directions to sections of a lightning
165 leader by analyzing the phase differences between antenna pairs for bursts of VHF pulse trains.
166 The triangulation of these spherical hyperbolas results in the 2D locations and occurrence times
167 of individual VHF sources [*Lojou et al.*, 2009]. The azimuthal precision of the sensors is
168 specified as ~0.5° RMS. The IC flash algorithm classifies each VHF source as part of an IC
169 stroke or, as an isolated IC source (also known as "singleton"; *Williams et al.*, 1999) according to
170 the distance and the time interval separating them. Each station LS8000 is also equipped with a
171 low frequency (LF) sensor to detect and locate the return strokes by using TOA/MDF technique,
172 which enables discrimination between IC and CG flashes. The DE for CG flashes estimated from
173 previous campaigns can be lower than ~80% for the domain considered in the present study
174 [*Pineda and Montanyà*, 2009].

175

176 2.3. Broadband EM emissions and charge moment changes

177 A system located at University of Bath (51.71N; 2.32W; ~1400 km from the storm location)
178 records broadband ELF/VLF/LF/MF electromagnetic waves. It consists of a metal plate insulated
179 from the ground to measure the vertical electric field, a precise GPS clock for timing the data
180 acquisition, and an analogue signal conditioning and digital data acquisition unit (*Füllekrug*,
181 2010). This instrument has the capability to record electric field magnitudes in the frequency
182 range from approximately ~4 Hz to ~400 kHz with a sampling frequency of 1 MHz, an
183 amplitude resolution of ~35 $\mu V\ m^{-1}$, and a timing accuracy of ~10-20 ns.

The current moment waveforms associated with the CG flashes [*Hu et al.*, 2002; *Cummer and Lyons*, 2005] are reconstructed from ELF receiver measurements, by using the method presented in detail by *Mlynarczyk et al.* [2015]. The ELF recordings are performed by the Hylaty ELF station in Poland [*Kulak et al.*, 2014]. The CMC and the iCMC for a CG lightning stroke are estimated by integrating the current moment waveform during the whole variation due to the lightning stroke and during its first 2 ms, respectively [*Cummer and Lyons*, 2005].

2.4. Cloud structure and characteristics

We use the Cloud Top Temperatures (CTT) provided by the Meteosat satellite from the European Organization for the Exploitation of Meteorological Satellites (EUMETSAT). The Meteosat Second Generation (MSG) Spinning Enhanced Visible and Infrared Imager (SEVIRI) is based on radiometer data in the thermal infrared band (IR) at ~11-13 μm. The temperature accuracy is generally better than ~1°. We take into account the parallax error (estimated to be about 15 km for a cloud top at ~12 km at this latitude) for the Figures that associate the locations of CG strokes with their parent clouds.

Observations performed by an AEMET network C-band (5 GHz) radar are used in the study. The radar is located in the Balearic Island of Mallorca (39.379ºN; 2.785ºE; emitter altitude ~111 m above mean sea level) and it is operated with a 10-minute cycle producing polar volumes. The configuration allows the retrieval of Doppler radial winds (DOW) and reflectivity (Z) under different modes of representation: (i) the Plan Position Indicator (PPI) that shows the distribution of the selected parameter on a constant elevation angle surface. (ii) Constant Altitude PPI (CAPPI) that consists in a horizontal "cut" at a selected altitude, generally used for surveillance and severe storm identification. (iii) Maximum reflectivity **(**MAX) that provides an easy-to-interpret presentation of the echo height and intensity in a single display. This product is calculated by first constructing a series of CAPPI's to span the selectable layer, and then determining the maximum data value for the horizontal projection. It is especially useful for depicting areas of severe weather.

3. Storm development and CG lightning activity

On 29 October 2013, a deep low of pressure system with a minimum at 975 hPa located over Northern Europe creates a trough in altitude over France and North of Spain and organized

a southeasterly flow that carries unstable air over northern Spain and the Mediterranean Sea. A CAPE value of ~1500 J kg^{-1} is reported from a sounding in Mallorca, Balearic Islands (39.606°N, 2.707°E) on 29 October at 0000 UT. *Romero et al.* [2015] analyzed in detail the conditions of development of the storm from observational to numerically simulated products. They showed the convection starts end of morning, entirely over the sea between the northeastern coastline of Spain and the Balearic Islands in the Mediterranean Sea, resulting from a progressive upper-level trough and the simultaneous advance of a surface cold front. The storm organized as a linear structure corresponding to a squall line, moves very fast over the Balearic Islands territory and more to the east at the end of the day with an indication of a possible transition into a bow-echo structure.

Figure 1a shows the lightning activity produced by this storm during its eastward propagation, with the location of two types of CG flashes (-CG and +CG) and the SP+CG strokes detected between 1000 UTC on 29 of October and 0400 UTC on 30 of October, separated in six time windows of three hours. Figure 1b-c displays the distribution of CTT at 1110 and 1610 UTC, respectively, that are the times of scanning of the area by the infrared radiometer (10.5/12.5 μm) onboard the MSG satellite. The CG lightning flashes detected by EUCLID during 10 minutes around the time of the scan are superimposed in this figure with white cross for –CG and red plus for +CG. The convective system propagates eastward with an average velocity of ~40 km h^{-1}. Figure 1b-c shows the growth of the cloud system simultaneously to its propagation during the first 6 hours of lightning activity. The coldest CTTs are -68°C and -73°C at 1110 and 1610 UTC, respectively. The majority of CG flashes are located in a restricted area that corresponds to the coldest CTT values, most likely related to the convective core of the storm. Some +CG flashes are scattered in the cloud structure when the storm system grows significantly in size. The thundercloud encompasses ~350 km × 350 km at 1610 UT and its propagation velocity is estimated at ~30 km h^{-1} for this first period of the storm activity.

Figure 2 displays the time series of the -CG and +CG flash rates, T_m the minimum of the CTT, A(-40) and A (-65) the areas of the cloud top with a temperature < -40°C and < -65°C, respectively, to estimate the cloud size and the size of the most convective regions. This evolution exhibits several features that allow us to distinguish four phases. First, between 1100 and ~1300 UTC the CG flash rate increases rapidly and reaches values around 15-20 fl min^{-1}, T_m

and A(-40) slowly increases, while A(-65) remains low. Secondly, between ~1300 and ~1600 UTC, T_m decreases up to its lowest value of -73°C, the CG flash rate increases continuously (especially the -CG), A(-40) increases more slowly and A(-65) increases markedly to reach its maximum at 1545 UTC. Then, between ~1600 and ~2000 UTC, the CG flash continues to increase and stabilizes around 25-30 fl min^{-1}, A(-40) increases very slowly and reaches its maximum value of ~140,000 km^2 at 1945 UTC, T_m becomes less cold, A(-65) fluctuates before to tend to zero at ~2000 UTC. After 2000 UTC the CG flash rate decreases, T_m increases, A(-65) stays close to zero while A(-40) decreases definitively. Thus, the storm storm has a faster growth during the first hours of its lifetime while the strongest convection characterized by A(-65) occurs between ~1300 and 2000 UTC.

4. Sprite observation

4.1. Overall storm activity

During the night between 1730 UTC and 0300 UTC, a large number of videos including sprite events are recorded by the camera located at Pic du Midi. During a first period between 1745 UTC and 1845 UTC when the storm centers at a longitude of ~4°E, the video imagery provides 22 videos, a video each 2.45 minutes on average. Some of these videos include several sprite elements associated with distinct SP+CG strokes, which enables a determination of ~32 stroke/sprite pairs during this first period. The reduced visibility at Pic du Midi because of cloudy conditions did not allow performing observations between 1842 UTC and 2130 UTC. A second period of sprite observations that starts at 2130 UTC provides 80 videos of sprite emissions above the same storm system, until 0240 UTC during its eastward displacement. The rate of sprite videos is especially high between 2200 and 2300 UTC with 38 detected sprites during about one hour i.e. one sprite each 1.5 minute. During this period ~~sequence~~, multiple sprite events are observed, with ~90 stroke/sprite pairs. Figure 1a displays the location of the SP+CG strokes detected by the lightning detection system EUCLID. The location clearly shows the two distinct periods of sprite observations and even though the second period is longer, the SP+CG strokes appear distributed on a smaller area.

We performed a detailed analysis of the lightning activity associated with two cases of sprite events, each one including several sequences of dancing sprites, issued from the first period of observation. During this period, the convective system was relatively close to our

observational capabilities, i.e. the lightning detection systems, the radar and the video camera. Figure 3 displays the CTT during two scans of Meteosat at 1810 UTC and 1825 UTC, two types of CG flash with white crosses and small red pluses for -CG and +CG, respectively, and the SP+CG strokes with large red pluses, all detected during 10 minutes around the scan time. The figure also displays the maximum radar reflectivity within the cloud system at 1810 UTC (c) and at 1820 UTC (d), detected with the radar in Mallorca. The cloud system is growing during the period of both scans and the coldest temperature is about -71°C. Most CG flashes occur in a small south-north elongated region of the cloud system corresponding to the coldest CTTs. This region is located between ~4.5°E-5°E of longitude and between ~38°E-39.5°E of latitude. The +CG flashes mainly occur in three groups, while the -CG flashes seem to be more uniformly distributed. The maximum radar reflectivity shows three cores of high reflectivity within the convective line with values between ~54-60 dBZ. The three cores correspond very well to areas with high negative and positive flash rates (Figure 3a-b). The SP+CG strokes are much more scattered than other CG flashes in the storm system. Indeed, out of the 21 SP+CG strokes included in both figures, 20 are far from the coldest part of the cloud top, i.e. up to 150 km for the farthest. The radar reflectivity map shows that the SP+CG strokes are located within a region exhibiting the typical structure of a stratiform region, as observed in many works [*Houze et al.*, 1990; *Carey et al.*, 2005; *Ely et al.*, 2008; *Lang et al.*, 2010; *Soula et al.*, 2009; *Lu et al.*, 2013]. Indeed, the maximum reflectivity is ~36-42 dBZ with a low horizontal gradient in the main part of the area. Several SP+CG strokes trigger sprites recorded in a same video as illustrated in more detail in the two following case studies.

4.2. Case of a series of dancing sprites at 18h03

Figure 4 illustrates the different phases of this multiple luminous event, the simultaneous lightning activity detected by different systems and the electromagnetic radiation recorded in various low frequency ranges. A graph displays the CTT pattern with the 2D location of the detections related to the lightning flash and lines of sight of the sprite elements from the camera. Other graphs display the time series of the optical events and lightning signals provided by the different instruments described in section 2. The caption of Figure 4 details the description of each graph. Table 2 provides time, location, current and discharge characteristics inferred from the signals produced by the luminous events and the associated lightning strokes.

307 The duration of this series of sprite sequences is ~1.76 s, i.e., 88 fields of 20 ms including
308 38 fields with sprite luminosity. The sprite event consists of four sequences of continuous light
309 emission, each one with duration ~120-220 ms, i.e., from 6 to 11 fields. Each of these sequences
310 starts after a SP+CG stroke with a varying delay. Figure 4a displays two fields from each
311 sequence, including the first field of each sequence. The images show that the horizontal extent
312 of successive sprite elements covers at least ~60 % of the FOV of the camera, i.e., ~18.5°. Figure
313 4b shows the SP+CG and the lines of sight following the same northeastward displacement. The
314 lines of sight inferred from the first fields of each sprite sequence (F1, F33, F62 and F82) match
315 very well with the SP+CG stroke locations, except the first one that is clearly shifted. The
316 distance between the first and last SP+CG is ~180 km by using the great circle path, which gives
317 an idea of the large extent of the lightning process during the 1.76 second long series of sprite
318 sequences.
319 During the first sprite sequence that starts with the longest delay ~62-82 ms (Table 2),
320 several elements are produced during ~200 ms and the first one (F1) is found at a distance of ~25
321 km with respect to the initial stroke at t = 8.829 s. Simultaneously to the sprite emission in F5,
322 locations of VHF radiation sources are mapped along the lines of sight in F5 (blue in Figure 4b
323 and upper graph of Figure 4c). There is a gap of ~0.44 s between the first sprite sequence and the
324 second that starts after a SP+CG stroke with a peak current of ~34 kA detected at t = 9.528 s.
325 Another gap of ~0.36 s whithout any recorded lightning activity precedes the third sprite
326 sequence associated with a SP+CG stroke of ~79 kA and a short delay followed by VHF sources
327 (yellow in Figure 4b-c). Figure 4b shows that the line of sight of the brightest element of the
328 sequence matches very well with the SP+CG stroke and the VHF emissions that follow it. After
329 a gap of ~0.2 s the fourth and shorter sprite sequence starts with a bright element after a SP+CG
330 stroke of ~152 kA and simultaneous VHF sources (orange in Figure 4b-c).
331 The 3-second long time series of the optical and lightning records in Figure 4c-d shows
332 that the four SP+CG strokes are identified in the electric field signal and that the larger the peak
333 current, the stronger the radiated electric field. The current moment waveform (red curve in
334 Figure 4c) shows clearly substantial current after the SP+CG strokes, either as a continuing
335 current after the second SP+CG stroke (green symbol) or as a surge after the other cases of
336 SP+CG strokes, either associated or not associated with VHF sources. These characteristics will
337 be discussed in more detail in Section 5.

4.3. Case of a series of dancing sprites at 18h08

Figure 5 displays the same set of measurements as in Figure 4, but for the second case of series of dancing sprites. The numerical values of the most important parameters are shown in Table 2. The second case consists of three sequences of continuous light emission spread over ~0.86 s, i.e., 43 fields of 20 ms including 33 fields with sprite luminosity. The duration of each sequence ranges from ~100 ms to ~320 ms, i.e., of 5 to 16 fields. Figure 5a displays one field for each of the two first sequences and six for the third sequence. The first sequence (F1-F5) starts between ~40 and ~60 ms after a SP+CG with a peak current of ~26 kA and a small increase of the electric field in central graph of Figure 5c (first red arrow). Figure 5b shows that F2 is ~30 km laterally displaced from the SP+CG location (light blue colour), which coincides with the line of sight of F17. The second sequence (F9-F20) is longer than the first one but still weakly luminous and no SP+CG stroke is detected prior to the sprite. However, a small electric field increase can be seen in central graph of Figure 5c (second red arrow) at t = 20.250 s, which indicates a lightning signal in the VLF/LF range that corresponds to the beginning of this sprite sequence. The third sprite sequence starts at t = 20.614 s, ~~and occurs~~ rapidly after a SP+CG stroke with a peak current of ~97 kA. After this stroke, the luminous sprite emission sustains relatively bright luminosity levels for ~280 ms associated with VHF activity detected in the same area (green colour), until a new SP+CG occurs at 20.899 s. This SP+CG stroke has a peak current of ~84 kA and triggers most of the luminous sprite elements visible in F40.

Figure 5b shows that the line of sight in F40 matches with the SP+CG stroke (yellow colour). The horizontal extent of the successive sprite elements covers ~60 % of the FOV of the camera, i.e., ~18.5°. The figure shows that the SP+CG and the lines of sight follow again a northeastward displacement. The distance between the first and last SP+CG is ~91 km. The three SP+CG strokes ~~detected~~ are identified in the electric field radiated in the VLF/LF range shown in both panels of Figure 5d, and the larger the peak current, the stronger the electric field. In the upper panel of Figure 5c, the current moment waveform (red curve) shows the discharge current between SP+CG strokes, in particular after the second stroke (green colour) associated with VHF sources. This sequence will be analyzed in Section 5.

5. Discussion

5.1. Storm characteristics during the sprite production

The storm that produces a large amount of sprites during the night of 29-30 October of 2013 develops in favorable synoptic conditions early in the day and moves eastward during all the day and a good part of the night while producing continuously large rates of lightning flashes. The conditions for sprite observation during the nocturnal period are met during two time intervals; the first interval lasts for only one hour because of the arrival of clouds around the camera. During this first period of sprite production, the cloud system is close to its maximum extent at about 140,000 km^2, as inferred from its CTT pattern issued from Meteosat images. The radar in Mallorca can cover at that time a large part of the storm system. At any moment of its lifetime, the large concentrations of CG flashes are located in the southern part of the cloud mass.

Figure 6 displays the horizontal distribution of the maximum reflectivity at a close time to the dancing sprites, i.e., at 1800 and 1810 UTC. The reflectivity highlights precipitation structures with convective cells within the cloud mass that correspond to the strong densities of CG flashes in a south-north oriented line and a large stratiform region northwest of the convective line. This stratiform region exhibits radar reflectivity lower than ~42 dBZ. Figure 7 displays the storm system with CTT (Figure 7a,b) and maximum radar reflectivity (Figure 7c,d), ~2 hours and ~1 hour earlier (Figure 7a,c and Figure 7b,d, respectively). It shows both convective and stratiform regions described above, the first one characterized by a large CG flash density and maximum values of reflectivity between 54 and 60 dBZ, the second one by very few CG flashes and maximum reflectivity values of ~42 dBZ. A line of some small cells is visible at 1710 UTC in the radar pattern, southwest from the stratiform region, but these cells do not produce any CG flash at that moment. The SP+CG strokes are mainly detected within the stratiform region, while very few CG flashes occur in it. Thus, during this first sprite period between about 1750 and 1840 UTC, the flash rate produced by the whole storm system is high but that of the storm structure really active for the sprite production is very low.

As illustrated in other studies, the convective region associated with the stratiform region in a sprite-producing MCS produces a lower flash rate when the sprites are observed [*Lang et al.*, 2010; *Soula et al.*, 2014; *Soula et al.*, 2015]. However, the correspondence between the convective activity and sprite occurrences can depend on the storm morphology as explained by *Lang et al.* [2010]. These authors considered two cases of sprite-producing storms, and found a

good correlation between convective intensity and sprite production, in a large and symmetric MCS that produced 282 sprites in 4 hours, while they observed an anti-correlation for an asymmetric storm that produced 25 sprites in 2 hours. However, in the first case most of SP+CG strokes were located in the stratiform region despite the strong correlation between convective intensity and sprite production. As noted by *Lyons* [2006] the more intense the storm system, the higher the sprite occurrence rate. In our case, the storm system produces a very high sprite rate between 2200 and 2300 UTC with 38 sprite videos, while the CG lightning flash rate decreases, the minimum CTT increases, and the spatial extent of the whole storm system decreases. This ~~sequence~~ period corresponds to the behaviour pointed by *Lang et al.* [2010] for the second example of storm. On the contrary, during the first sprite period of sprite production (1748 UTC – 1842 UTC), the convective intensity is high with CTT lower than -40°C because of a region of the storm, independent of the stratiform region concerned by the sprite production, as illustrated in Figure 3. This period ~~sequence~~ corresponds to the first storm described by *Lang et al.* [2010].

5.2. Lightning/Sprite timing and location

In both cases of ~~the~~ dancing sprites series, a similar behaviour is observed. The sprite event starts with a SP+CG stroke that triggers several sprite elements ~~that appear to~~ propagating north-eastward and followed by new pairs SP+CG stroke/sprite elements that also ~~appear to~~ propagate north-eastward ~~inside/above the cloud system~~. The simultaneous propagation of both events, the SP+CG stroke and the sprite elements, is observed across the stratiform region. Indeed, Figure 6 indicates the locations of the SP+CG strokes relative to the precipitation detected by the radar. In both cases, the dual discharge phenomenon (stroke/sprite) crosses the stratiform region, from a convective region with small convective cells, up to the opposite end of the storm system. It seems that this progression of the discharge processes follows a pattern, i.e., the initial discharge is close to the region of the storm where convective cells are located, and subsequently, the leader processes propagate to the stratiform region as shown by VHF sources detected by the XDDE.

Similar observations were made in several studies based on LMA detections [*Lang et al.*, 2010; *Lu et al.*, 2013; *van der Velde et al.*, 2014, *Soula et al.*, 2015]. However, in both series of ~~the~~ dancing sprites reported here, ~~the~~ VHF sources are not continuously detected between the areas where the SP+CG strokes are located or between the lines of sight where the sprite

elements are observed. We have to keep in mind the XDDE interferometer does not map leaders as the LMA does. *Mazur et al.* [1997] compared data from two systems that detected VHF radiations produced by storms in Florida. One of the systems, the LDAR that uses the TOA technique, showed continuity in time and a three-dimension structure of radiation sources. On the contrary, the data from an interferometric system equivalent to the XDDE were more intermittent in time and had a ~~more~~ two dimensional structure. In the present study, the extension and the duration (up to ~180 km and 1.76 s, respectively, for the sprite event at 1803 UTC) of the lightning processes associated with both sprite events seem consistent with the three cases of spider lightning flashes described by *Mazur et al.* [1998]. Indeed according to this description, they occurred in the stratiform region of decaying storms and consisted of negative leaders propagating over several tens of kilometres with a speed of 2-4 10^5 m s^{-1}. Furthermore, one of them lasted 2.4 s. According to these authors, the interferometer cannot map this kind of negative leader when several branches develop simultaneously which could explain the discontinuity of the VHF source production in the present cases. In both cases of multiple-sequence dancing sprites, the most luminous elements occur at the end of the event, i.e. when the SP+CG is far from the convective region.

5.3. Lightning stroke current and sprite relationships

According to Table 2, each sprite sequence starts with a delay significantly larger than 40 ms (>62 ms for one and >40 ms for the other) that can be considered as a long time-delayed [*Lu et al.*, 2013]. ~~luminous emission, one with a delay >60 ms and another with a delay >40 ms~~. Furthermore, the first sprite elements of each event are seen to be more shifted from the SP+CG stroke, than the following elements. As indicated by *Lu et al.* [2013] we observe that the long time-delayed sprites are more significantly displaced from the parent stroke. The iCMC of the lightning stroke at the origin of the first sprite sequence at 1803 UTC has a value as low as 174 C km. The iCMC of the first SP+CG stroke for the second sprite sequence at 1808 UTC cannot be calculated. For the successive sprite emissions in each sequence a common behaviour appears, i.e., the shorter delays (< 15 ms) correspond to the larger values of the iCMC (> 400 C km). The same observation was reported in *Lu et al.* [2013] from a set of 26 flashes producing sprites above an asymmetric MCS. In addition, the larger values of iCMC produce the brightest sprite elements, typically in fields F82 and F41 for the sprites at 1803 and 1808 UTC, respectively.

462 This finding is similar to that in *Soula et al.* [2015] for several triangulated sprites in
463 southeastern France, insofar as the long delayed sprites are produced after a positive stroke with
464 a low value of iCMC.

465 The brightest sprite elements (F82 and F41) correspond also to large CMC values for the
466 SP+CG strokes, 6935 C km and 5277 C km, respectively) ~~and to large values of iCMC (839 C~~
467 ~~km and 440 C km, respectively)~~, as indicated in Table 2. As in *Yaniv et al.* [2014], the brightness
468 is correlated with the CMC value of the parent stroke. However, in the present case, the first
469 sprite element for the case at 1803 UTC is produced with a long delay after a SP+CG stroke with
470 a very large value of CMC (~5000 C km calculated over ~60 ms after the stroke which
471 corresponds to the first field with sprite luminosity F1) as shown in Figure 8a. Indeed, the panel
472 with the current moment waveform shows a current pulse at 1803:8.829 UTC (t = 0 in Figure
473 8a), i.e., ~60 ms before F1~~, the first field with sprite luminosity~~. According to the current
474 moment waveform, the discharge continues during a few tens of ms that may correspond to a
475 lightning continuing current. An increase of current starts at 1803:8.829 UTC (t = 100 ms in
476 Figure 8a), lasts a few tens of milliseconds and corresponds to the fields F3, F4 and F5 with new
477 sprite elements with the shape of carrot sprites. Thus, the current produced can be due to
478 lightning processes that sufficiently discharges the cloud to produce new sprite elements,
479 especially as VHF sources are detected by the XDDE system along the line of sight of F5 as
480 indicated in Figure 4b,c. It could be also produced by the sprite itself, but it seems more
481 consistent with a current waveform due to M-components superimposed to a long continuing
482 current, as observed by *Lu et al.* [2013] for a dancing sprite. This observation is quite consistent
483 with the study by *Li et al.* [2008] about delayed sprites. Their data showed that 46% of the sprite
484 elements were triggered with a delay larger than 10 ms after the SP+CG strokes and associated
485 with a substantial continuing current. Furthermore, these authors found that an intensification of
486 the continuing current can play a major role in the sprite triggering and that the sferic burst
487 simultaneously recorded is another consequence of the current intensification.

488 Figure 8b displays the current moment waveform and the CMC for another period of
489 ~600 ms during the sprite series ~~sequence~~ at 1803 UTC. In this case, the bright sprite element
490 (F82) is produced with a short delay after the stroke at 1803:10.516 UTC (t = 0 in Figure 8b).
491 The current pulse of this stroke is followed by a current signature 100 ms long that may

correspond to a continuing current and that includes a current pulse ~60 ms after that stroke and a new sprite element is detected in F85 in the form of a carrot sprite that is still bright in F86. In this case, no VHF source is detected by the XDDE system after the stroke, but we can infer that the current intensification is due to a M-component superimposed to the continuing current that triggers the sprite elements in F85-F86. We cannot exclude the sprite itself makes a contribution to the current signature. By comparing the sprite elements in F85 to those visible in F82, their structure seems vertically different. Actually at the location of two bright bodies of sprite elements at about 70 and 75 km in F82-F84 (b_1 and b_2 in Figure 8b) the new sprite elements in F85 and F86 exhibit a diffuse cap (c'_1 and c'_2, respectively) while their bright body develops at a lower altitude, 60-65 km (b'_1) and 55-65 km (b'_2), respectively, ~~at the location of filaments from the previous sprite elements~~. Thus, several characteristics of these new carrot sprite elements in F84 – their simultaneity with the current surge during the continuing current following the SP+CG stroke and their common lines of sight with sprite elements issued from the first and bright elements following the SP+CG stroke (t = 0 in Figure 8b) – suggest an initiation favoured by the local change of the conductivity due to the initial sprite elements. ~~reach the altitude of the ionosphere appear as a reillumination of the previous ones with a larger size and a different structure.~~ Since these new sprites correspond to carrot elements, their extension at lower altitude is consistent with the observations by *van der Velde* [2008] and *Stenbaek-Nielsen et al.* [2010] that show carrots start at a lower altitude and develop upward streamers from the body for 10-15 km. This assumption is supported by the horizontal alignment of initial and new streamers all the more so the initial ones last for several fields (F82-F84) and therefore the electric field is maintained during the same time interval. The discharge process indicated by the current surge during the continuing current can reinforce this electric field and trigger new streamers. However, because the sprite elements are not triggered, we cannot conclude definitively that the different streamers correspond at the same region. Thus, as in *Li et al.* [2008], we observe an altitude a few kilometres lower for the delayed sprites, triggered a few tens of milliseconds after previous sprites. ~~We can suppose the initial elements change the conductivity locally and probably the potential since the initial sprite elements reach the altitude of the ionosphere (Figure 8b), which allows new sprite elements to develop following the surge visible in the current moment waveform simultaneous to F85. Indeed, the conditions to trigger secondary TLEs may be favourable if the altitude of the ionosphere potential is lowered after a preceding sprite and~~

~~when a high concentration of charge is present in the thundercloud, as explained by *Marshall and Inan* [2007], *Lee et al.* [2012]. These sprite elements could be then considered as secondary sprites, as described in *Mlynarczyk et al.* [2015] for a secondary TLE of troll-type in a case of dancing sprite. *Li et al.* [2008] observed also an altitude a few kilometres lower for the delayed sprites, triggered a few tens of milliseconds after previous sprites.~~

Figure 9 displays the current moment waveform and the CMC for another case of sprite with a long light emission after a SP+CG stroke at 1808:20.626 UTC. Six fields out of nine over a period of 180 ms show the light emission. After the field associated with the SP+CG stroke (F27), two other fields exhibit re-enforced light (F30 and F35) and correspond each one with an increase of the current moment waveform, at about t = 50 ms and t = 150 ms after 1808:20.626 UTC. No lightning stroke was detected by the different systems, between F27 and F35 (180 ms), as indicated in Figure 5. However, the XDDE system recorded VHF activity, especially during the first 50 ms after 1808:20.626 UTC and more sporadically up to 1808:20.899 UTC, when a new SP+CG stroke triggers the brightest sprite of the event. Likewise for this case, both current moment waveform and light emission correlate very well. The delayed sprite elements in F35 appear clearly at a lower altitude compared to the previous sprite elements in F27 and in F30. Indeed, the bright body of the sprite elements appear successively at altitudes around 70 km in F27, between 60 and 70 km in F30 and between 50 and 60 km in F35. This observation also illustrates the observation made by *Li et al.* [2008]. ~~These observations gives substance to the explanation by *Lee et al.* [2012] that argues a lowering of the altitude of the ionosphere potential to assist to trigger consecutive TLEs.~~ Recent theories suggest that mesospheric irregularities might be a necessary condition for the initiation of sprite streamers [*Liu et al.*, 2012; *Kosar et al.*, 2012; *Qin et al.*, 2014], and that the sprite streamers can produce low-frequency electromagnetic radiation [*Qin et al.*, 2012; *Füllekrug et al.*, 2013b]. Our observations of delayed sprites associated to current surges during the continuing current and following initial sprite elements can support this theory.

5.4. Sprite current signature

Previous studies reported pulse-shaped current signature related to sprites, in particular when they are very bright [*Cummer et al.*, 1998; *Füllekrug et al.*, 2001; *Hu et al.*, 2008; *Soula et al.*, 2014; *Mlynarczyk et al.*, 2015]. Figure 10 displays the electric field radiated in ELF/VLF/LF

(upper/central/lower graphs) during 120 ms, 25 ms before and 95 ms after the SP+CG in both cases of series of dancing sprites: a) at 1803:10.123 UTC that corresponds to the brightest sprite element in F62 of Figure 4a; b) at 1808:20.899 UTC that corresponds to the brightest sprite element in F40 of Figure 5a. Current signatures are ~~clearly~~ visible in the upper graph of Figures 10a and 10b, a few milliseconds after the ELF pulses produced by the SP+CG return strokes, that corresponds to t = 5 ms in the graphs (t = 10.123 s and t = 20.899 s, respectively). The time intervals between the SP+CG pulse and this current pulse ~~that of the sprite~~ are consistent with the values of Δt issued from Table 1 for both cases, since they are included within [0 - 8 ms] and [0 - 15 ms], respectively. These current pulses observed in ELF range only, similar to the signatures shown in *Cummer et al.* [1998] and *Soula et al.* [2014] with a short duration of about ~2-3 ms, can be attributed to sprites. They can also last longer times as observed for example in *Mlynarczyk et al.* [2015] and *Füllekrug et al.* [2001] with a few tens of milliseconds. Figure 11 displays three cases of current moment change for three SP+CG strokes, each associated with a bright and short time-delayed sprite. We can clearly distinguish the sprite current in Figure 11c, less clearly in Figure 11a and not at all in Figure 11b. It seems that the impulsive current from the sprite itself can overlap with the current from the parent stroke if the delay after the trigger is very short (< 2ms) such that the sprite current remains obscured.

6. Conclusion

We consider data relative to different aspects of the activity of a storm that produced a large number of sprite events, especially to analyze two series of sprite sequences that strongly resemble to dancing sprites. The dataset includes optical emissions recorded by a low-light video camera, characteristics of the CG strokes (time, location, peak current, CMC calculated from ELF signals and current moment waveform), VHF radiations relative to the lightning flashes, electric field radiated by lightning flashes in a large band of low frequencies, ~~CMC calculated from ELF signals, current moment waveform,~~ CTT issued from the radiometer onboard the MSG satellite, and fields of the maximum radar reflectivity. The storm starts at the end of the morning over Mediterranean Sea close to northeastern Spanish coastline, then moves eastward during its lifetime estimated at ~18 hours. The CG lightning flash rate of this storm reaches more than 30 fl min^{-1}, while the CTT reaches a minimum value of -73°C at ~1600 UTC. The size of this storm system reaches 140,000 km^2 by considering the region with a CTT <-40°C. We analyze in detail

584 the complex structure of the storm and the lightning activity associated with sprites recorded
585 during a first period ~~sequence~~ of production at the beginning of the night. At that moment, the
586 region of the storm involved in the sprite production is around 400 km from the camera that
587 records several sprite events including dancing sprites. ~~Furthermore,~~ We analyze in detail two
588 series of successive sequences of dancing sprites, one of both with a duration exceeding 1
589 second.

590 Several results can be put forward from this case study: (i) The first period of sprite
591 production is clearly associated with a region of the storm system characterized by a stratiform
592 structure and a very low CG lightning flash rate. (ii) For each series of dancing sprites analyzed,
593 the luminous emissions repeat the timing and the location of several lightning strokes spread
594 along the stratiform region of the storm. (iii) The brightest sprite elements produce significant
595 current signatures a few milliseconds (< 5 ms) after the parent stroke, visible if the delay is not
596 too short. (iv) Long time-delayed sprite elements correspond to low values of iCMC of the parent
597 strokes and most of time they are associated with surges in the current moment waveform during
598 the continuing current. (v) Several of these long time-delayed sprite elements trigger after a
599 previous short time-delayed sprite and apparently at a lower altitude. ~~The lowering of the~~
600 ~~ionosphere potential by the previous sprite could explain this observation~~.
601
602 **Acknowledgments.** The authors thank Themis Chronis and two anonymous reviewers for their
603 valuable comments in the evaluation of the paper. The authors thank the company Meteorage
604 and the Danish Technical University, for their help to provide the CG lightning activity data.
605 Observations and studies about TLEs made by SS and JFG were partly sponsored by the
606 National Institute of Universe Science (INSU) thanks to LEFE/IMAGO. The work of MF is
607 sponsored by the Natural Environment Research Council (NERC) under grants NE/L012669/1
608 and NE/H024921/1. JM has been supported by the National Science Centre under grant
609 2015/19/B/ST10/01055. The contribution of Spanish participants to the study was supported by
610 research grants from the Spanish Ministry of Economy and Competitiveness (MINECO) and
611 European Regional Development Fund (ERDF): AYA2011-29936-C05-04, ESP2013-48032-C5-
612 3-R and ESP2015-69909-C5-5-R. All data used in this paper can be requested from the
613 corresponding author at serge.soula@aero.obs-mip.fr.
614

615

616 **References**

617 Bell, T. F., S. C. Reising, and U. S. Inan (1998), Intense continuing currents following
618 positive cloud-to-ground lightning associated with red sprites, *Geophys. Res. Lett., 25*(8), 1285–
619 1288, doi:10.1029/98GL00734.

620 Boccippio, D. J., E. R. Williams, S. J. Heckman, W. A. Lyons, I. Baker, and R. Boldi
621 (1995), Sprites, ELF transients and positive ground strokes, *Science, 269*, 1088-1091.

622 Boeck, W.L., O.H. Vaughan, R.J. Blakeslee, B. Vonnegut, M. Brook, and J. McKune
623 (1994), Observations of lightning in the stratosphere, *J. Geophys. Res., 100*(D1), 1465–1475,
624 doi: 10.1029/94JD02432

625 Bór, J. (2013), Optically perceptible characteristics of sprites observed in central Europe
626 in 2007–2009, *J. Atmos. Sol.-Terr. Phys., 92*, 151–177, doi:10.1016/j.jastp.2012.10.008.

627 Carey, L. D., M. J. Murphy, T. L. McCormick, and N. W. S. Demetriades (2005),
628 Lightning location relative to storm structure in a leading-line, trailing-stratiform mesoscale
629 convective system, *J. Geophys. Res., 110*, D03105, doi:10.1029/2003JD004371.

630 Chen, A.B., et al. (2008), Global distributions and occurrence rates of transient luminous
631 events, *J. Geophys. Res. 113*, A08306. http://dx.doi.org/10.1029/2008JA013101.

632 Cummer, S. A., and M. Füllekrug (2001), Unusually intense continuing current in
633 lightning produces delayed mesospheric breakdown, *Geophys. Res. Lett., 28*(3), 495-498,
634 doi:10.1029/2000GL012214.

635 Cummer, S. A., and W. A. Lyons (2005), Implications of lightning charge moment
636 changes for sprite initiation, *J. Geophys. Res., 110*, A04304, doi:10.1029/2004JA010812.

637 Cummins, K. L., and M.J. Murphy (2009), An overview of lightning locating systems:
638 History, techniques, and data uses, with an in-depth look at the U.S. NLDN, *IEEE Trans.*
639 *Electromagn. Compat. 51*, 3, 499-518.

640 Cummins, K. L., M. J. Murphy, E. A. Bardo, W. L. Hiscox, R. B. Pyle, and A. E. Pifer
641 (1998), NLDN'95, A combined TOA/MDF technology upgrade of the US National Lightning
642 Detection Network, *J. Geophys. Res., 103*, 9035–9044.

643 Ely, B. L., R. E. Orville, L. D. Carey, and C. L. Hodapp (2008), Evolution of the total
644 lightning structure in a leading-line, trailing stratiform mesoscale convective system over
645 Houston, Texas, *J. Geophys. Res., 113*, D08114, doi:10.1029/2007JD008445.

Franz, R. C., R. J. Nemzak, and J. R. Winkler (1990), Television image of a large upward electrical discharge above a thunderstorm system, *Science, 249*, 48–51.

Fukunishi, H., Y. Takahashi, A. Uchida, M. Sera, K. Adachi, R. Miyasato (1999), Occurrences of sprites and elves above the Sea of Japan near Hokuriku in Winter, *EOS, 80*(46), F217.

Füllekrug, M., (2010), Wideband digital low-frequency radio receiver, *Meas. Sci. Technol. 21*, 015901. http://dx.doi.org/10.1088/0957-0233/21/1/015901.

Füllekrug, M., D. R. Moudry, G. Dawes, and D. D. Sentman (2001), Mesospheric sprite current triangulation, *J. Geophys. Res., 106*(D17), 20,189–20,194, doi:10.1029/2001JD900075.

Füllekrug M., A. Mezentsev, S. Soula, O. van der Velde, and T. Farges (2013a), Sprites in low-frequency radio noise, *Geophys. Res. Lett., 40*, 2395–2399, doi:10.1002/grl.50408.

Füllekrug M., A. Mezentsev, S. Soula, O. van der Velde, and A. Evans (2013b), Illumination of Mesospheric Irregularity by Lightning Discharge, *Geophys. Res. Lett., 40*(24), 6411-6416, doi: 10.1002/2013GL058502.

Houze, R. A., Jr., B. F. Smull, and P. Dodge (1990), Mesoscale organization of springtime rainstorms in Oklahoma, *Mon. Weather Rev., 118*, 613‑654, doi:10.1175/1520-0493(1990)118<0613:MOOSRI>2.0.CO;2.

Hu, W., S. A. Cummer, and W. A. Lyons (2007), Testing sprite initiation theory using lightning measurements and modeled electromagnetic fields, *J. Geophys. Res., 112*, D13115, doi:10.1029/2006JD007939.

Kosar, B., N. Liu, and H. Rassoul (2012), Luminosity and propagation characteristics of sprite streamers initiated from small ionospheric disturbances at subbreakdown conditions, *J. Geophys. Res., 117*(A8), A08328, doi:10.1029/2012JA017632.

Kulak, A., J. Kubisz, S. Klucjasz, A. Michalec, J. Mlynarczyk, Z. Nieckarz, M. Ostrowski, and S. Zieba (2014), Extremely low frequency electromagnetic field measurements at the Hylaty station and methodology of signal analysis, *Radio Sci., 49*, 361–370, doi:10.1002/2014RS005400.

Lang, T. J., S. A. Rutledge, and K. C. Wiens (2004), Origins of positive cloud-to-ground lightning flashes in the stratiform region of a mesoscale convective system, *Geophys. Res. Lett., 31*, L10105, doi:10.1029/2004GL019823.

Lang, T. J., W.A. Lyons, S.A. Rutledge, J. D. Meyer, D. R. MacGorman, and S. A. Cummer (2010), Transient luminous events above two mesoscale convective systems: Storm structure and evolution, *J. Geophys. Res.*, *115*, A00E22, doi:10.1029/2009JA014500.

~~Lee, L. J., S. M. Huang, J. K. Chou, C. L. Kuo, A. B. Chen, H. T. Su, R. R. Hsu, H. U. Frey, Y. Takahashi, and L. C. Lee (2012), Characteristics and generation of secondary jets and secondary gigantic jets, *J. Geophys. Res.*, *117*, A06317, doi:10.1029/2011JA017443.~~

Li, J., S. A. Cummer, W. A. Lyons, and T. E. Nelson (2008), Coordinated analysis of delayed sprites with high‐speed images and remote electromagnetic fields, *J. Geophys. Res.*, *113*, D20206, doi:10.1029/2008JD010008.

Li, J., and S. A. Cummer (2009), Measurement of sprite streamer acceleration and deceleration, *Geophys. Res. Lett.*, *36*, L10812, doi:10.1029/2009GL037581.

Liu, N., B. Kosar, S. Sadighi, J. R. Dwyer, and H. K. Rassoul (2012), Formation of streamer discharges from an isolated ionization column at subbreakdown conditions, *Phys. Rev. Lett.*, *109*, 025002, doi:10.1103/PhysRevLett.109.025002.

Lojou, J.Y., Murphy, M.J., Holle, R.L., Demetriades, N.W. (2009), Nowcasting of thunderstorms using VHF measurements. In: Betz, H.-D., Schumann, U., Laroche, P. (Eds.), Lightning: principles, Instruments and Applications. Springer, pp. 253–270.

Lu, G., et al. (2013), Coordinated observations of sprites and in-cloud lightning flash structure, *J. Geophys. Res. 118*, 6607–6632, doi:.10.1002/jgrd.50459.

Lyons, W. A. (1994), Low-light video observations of frequent luminous structures in the stratosphere above thunderstorms, *Mon. Wea. Rev.*, *122*, 1940–1946.

Lyons, W. A. (1996), Sprite observations above the U.S. High Plains in relation to their parent thunderstorm systems, J. Geophys. Res., 101(D23), 29,641-29,652.

Lyons, W. A., T. E. Nelson, E. R. Williams, J. A. Cramer, and T. R. Turner (1998), Enhanced positive cloud-to-ground lightning in thunderstorms ingesting smoke from fires, Science, 282, 5386, doi:10.1126/science.282.5386.77.

Lyons, W. A., T. E. Nelson, E. R. Williams, S. A. Cummer, and M. A. Stanley (2003), Characteristics of sprite-producing positive cloud-to-ground lightning during the 19 July 2000 STEPS mesoscale convective systems, *Mon. Weather Rev.*, *131*, 2417.

~~Marshall, R. A., and U. S. Inan (2007), Possible direct cloud-to-ionosphere current evidenced by sprite-initiated secondary TLEs, *Geophys. Res. Lett.*, *34*, L05806, doi:10.1029/2006GL028511.~~

Mazur, V., E. Williams, R. Boldi, L. Maier, and D. E. Proctor (1997), Initial comparison of lightning mapping with operational time-of-arrival and interferometric systems, *J. Geophys. Res.*, *102*(D10), 11,071‑11,086, doi:10.1029/97JD00174.

Mazur, V., X. Shao, and P. R. Krehbiel (1998), "Spider" lightning in intracloud and positive cloud-to-ground flashes, *J. Geophys. Res.*, *103*(D16), 19,811–19,822, doi:10.1029/98JD02003.

Mlynarczyk, J., J. Bór, A. Kulak, M. Popek, and J. Kubisz (2015), An unusual sequence of sprites followed by a secondary TLE: An analysis of ELF radio measurements and optical observations, *J. Geophys. Res. Space Physics*, *120*, 2241–2254, doi:10.1002/2014JA020780.

Montanyà, J., O. van der Velde, D. Romero, V. March, G. Solà, N. Pineda, M. Arrayas, J. L. Trueba, V. Reglero, and S. Soula (2010), High-speed intensified video recordings of sprites and elves over the western Mediterranean Sea during winter thunderstorms, *J. Geophys. Res.*, *115*, A00E18, doi:10.1029/2009JA014508.

Moudry D., H. Stenbaek-Nielsen, D. Sentman, E. Wescott (2003), Imaging of elves, halos and sprite initiation at 1 ms time resolution, *J. Atmos. Sol. Terr. Phys. 65*, 509–518. doi:10.1016/S1364-6826(02)00323-1.

McHarg, M. G., R. K. Haaland, D. Moudry, and H. C. Stenbaek-Nielsen (2002), Altitude-time development of sprites, *J. Geophys. Res.*, *107*(A11), 1364, doi:10.1029/2001JA000283.

Neubert T., T.H. Allin, H. Stenbaek-Nielsen, E. Blanc (2001), Sprites over Europe. *Geophys. Res. Lett.* 28:3585, doi:10.1029/2001GL013427.

Neubert T., M. Rycroft, T. Farges, E. Blanc, O. Chanrion, E. Arnone, A. Odzimek, N. Arnold, C.-F. Enell, E. Turunen, T. Bösinger, Á. Mika, C. Haldoupis, R. J. Steiner, O. van der Velde, S. Soula, P. Berg, F. Boberg, P. Thejll, B. Christiansen, M. Ignaccolo, M. Füllekrug, P. T. Verronen, J. Montanyà, and N. Crosby (2008), Recent Results from Studies of Electric Discharges in the Mesosphere, *Surveys in Geophysics*, 10.1007/s10712-008-9043-1.

Pasko, V. P., U. S. Inan, T. F. Bell, and Y. N. Taranenko (1997), Sprites produced by quasi-electrostatic heating and ionization in the lower ionosphere, *J. Geophys. Res.*, *102*(A3), 4529-4561, doi:10.1029/96JA03528.

736 Pineda, N., and J. Montanyà (2009), Lightning detection in Spain: the particular case of
737 Catalonia. Lightning: Principles, Instruments and Applications. Betz, H.-D., Schumann, U.,
738 Laroche, P. (Eds.), Springer, Netherlands: 161-185.
739 Pinto, O., Jr., M. M. F. Saba, I. R. C. A. Pinto, F. T. São Sabbas, K. P. Naccarato, M. J.
740 Taylor, P. D. Pautet, and R. H. Holzworth (2004), Thunderstorm and lightning characteristics
741 associated with sprites in Brazil, *Geophys. Res. Lett., 31*, L13103, doi:10.1029/2004GL020264.
742 Poelman, D. R., W. Schulz, G. Diendorfer, and M. Bernardi (2016), The European
743 lightning location system EUCLID – Part 2: Observations, *Nat. Hazards Earth Syst. Sci., 16*,
744 607-616, doi:10.5194/nhess-16-607-2016.
745 Qin, J., S. Celestin, and V. Pasko (2012), Minimum charge moment change in positive
746 and negative cloud to ground lightning discharges producing sprites, *Geophys. Res. Lett., 39*
747 (22), L22801, doi:10.1029/2012GL053951.
748 Qin, J., S. Celestin, and V. P. Pasko (2013), Dependence of positive and negative sprite
749 morphology on lightning characteristics and upper atmospheric ambient conditions, *J. Geophys.*
750 *Res. Space Physics, 118*, 2623–2638, doi:10.1029/2012JA017908.
751 Romero, R., C. Ramis, and V. Homar, (2015), On the severe convective storm of 29
752 October 2013 in the Balearic Islands: observational and numerical study, *Q. J. Roy. Meteorol.*
753 *Soc., 141*, 1208–1222, doi:10.1002/qj.2429.
754 São Sabbas, F. T., D. D. Sentman, E. M. Wescott, O. Pinto Jr., O. Mendes Jr., and M. J.
755 Taylor (2003), Statistical analysis of space-time relationships between sprites and lightning, *J.*
756 *Atmos. Solar-Terr. Phys., 65*, 525-535.
757 São Sabbas, F. T., M. J. Taylor, P. D. Pautet, M. Bailey, S. Cummer, R.R. Azambuja, J.
758 P. C. Santiago, J. N. Thomas, O. Pinto, N. N. Solorzano, N. J. Schuch, S. R. Freitas, N. J.
759 Ferreira, J. C. Conforte (2010), Observations of prolific transient luminous event production
760 above a mesoscale convective system in Argentina during the Sprite2006 Campaign in Brazil, *J.*
761 *Geophys. Res., 115*, A00E58, doi:10.1029/2009JA014857.
762 Sentman, D. D., and E. M. Wescott (1993), Observations of upper atmospheric optical
763 flashes recorded from an aircraft, *Geophys. Res. Lett., 20*(24), 2857-2860,
764 doi:10.1029/93GL02998.

765 Sentman, D. D., E. M. Wescott, D. L. Osborne, D. L. Hampton, and M. J. Heavner
766 (1995), Preliminary results from the Sprites94 Aircraft Campaign: 1. Red sprites, *Geophys. Res.*
767 *Lett., 22*(10), 1205-1208, doi:10.1029/95GL00583.
768 Soula, S., O. van der Velde, J. Montanyà, T. Neubert, O. Chanrion, and M. Ganot (2009),
769 Analysis of thunderstorm and lightning activity associated with sprites observed during the
770 EuroSprite campaigns: Two case studies, *Atmos. Res., 91*, 2-4, pp 514-528,
771 doi:10.1016/j.atmosres.2008.06.017.
772 Soula, S., O. van der Velde, J. Palmieri, J. Montanya, O. Chanrion, T. Neubert , F.
773 Gangneron, Y. Meyerfeld, F. Lefeuvre, and G. Lointier (2010), Characteristics and conditions of
774 production of transient luminous events observed over a maritime storm, *J. Geophys. Res., 115*,
775 D16118, doi:10.1029/2009JD012066.
776 Soula, S. and J.F. Georgis (2013), Surface electrical field evolution below the stratiform
777 region of MCS storms, *Atmos. Res., 132–133*, pp 264-277, DOI:
778 10.1016/j.atmosres.2013.05.008.
779 Soula, S., F. Iacovella, O. van der Velde, J. Montanyà, M. Füllekrug, T. Farges, J. Bór, J.-
780 F. Georgis, S. NaitAmor, and J.-M. Martin (2014), Multi-instrumental analysis of large sprite
781 events and their producing storm in southern France, *Atmos. Res., 135*, 415-431,
782 10.1016/j.atmosres.2012.10.004.
783 Soula, S., et al. (2015), Time and space correlation between sprites and their parent
784 lightning flashes for a thunderstorm observed during the HyMeX campaign, *J. Geophys. Res.*
785 *Atmos., 120*, 11,552–11,574, doi:10.1002/2015JD023894.
786 Stanley M., P. Krehbiel, M. Brook, C. Moore, W. Rison, B. Abrahams (1999), High
787 speed video of initial sprite development, *Geophys. Res. Lett. 26*:3201.
788 doi:10.1029/1999GL010673.
789 Stenbaek-Nielsen, H. C., and M. G. McHarg (2008), High time-resolution sprite imaging:
790 Observations and implications, *J. Phys. D Appl. Phys., 41*, 234009.
791 Stenbaek-Nielsen, H. C., R. Haaland, M. G. McHarg, B. A. Hensley, and T. Kanmae
792 (2010), Sprite initiation altitude measured by triangulation, *J. Geophys. Res., 115*, A00E12,
793 doi:10.1029/2009JA014543.

Su, H. T., R. R. Hsu, A. B. Chen, Y. J. Lee, and L C. Lee (2002), Observations of sprites over the Asian continent and over oceans around Taiwan, *Geophys. Res. Lett., 29*(4), 1044, doi:10.1029/2001GL013737.

van der Velde, O.A. (2008), Morphology of sprites and conditions of sprite and jet production in mesoscale thunderstorm systems, *PhD thesis*, University Paul Sabatier, Toulouse.

van der Velde, O. A., Á. Mika, S. Soula, C. Haldoupis, T. Neubert, and U. S. Inan (2006), Observations of the relationship between sprite morphology and in-cloud lightning processes, *J. Geophys. Res., 111*, D15203, doi:10.1029/2005JD006879.

van der Velde, O. A., J. Montanya, S. Soula, N. Pineda, and J. Bech (2010), Spatial and temporal evolution of horizontally extensive lightning discharges associated with sprite-producing positive cloud-to-ground flashes in northeastern Spain, *J. Geophys. Res., 115*, A00E56, doi:10.1029/2009JA014773.

van der Velde, O. A., J. Montanya, S. Soula, N. Pineda, and J. Mlynarczyk (2014), Bidirectional leader development in sprite-triggering lightning flashes, *J. Geophys. Res. Atmos., 119*, doi:10.1002/2013JD021291.

Vaughan, Jr., O. H., R. J. Blakeslee,W. L. Boeck, B. Vonnegut, M. Brook, and J. McKune Jr. (1992), A cloud-to-space lightning as recorded by the space shuttle payload-bay TV cameras, *Mon. Weather Rev., 120*, 1459–1461.

Williams, E.R. (2001), Sprites, elves, and glow discharge tubes, *Physics Today, 54*(11), 41-47.

Williams, E., B. Boldi, A. Matlin, M. Weber, S. Hodanish, D. Sharp, S. Goodman, R. Raghavan, D. Buechler, (1999), The behavior of total lightningactivity in severe Florida thunderstorms, *Atmos. Res., 5*, 1245–1265.

Winckler, J. R., W. A. Lyons, T. E. Nelson, and R. J. Nemzek (1996), New high-resolution ground-based studies of sprites, *J. Geophys. Res., 101*(D3), 6997-7004, doi:10.1029/95JD03443.

Yang J., X. Qie, G. Zhang, Y. Zhao, T. Zhang (2008), Red sprites over thunderstorms in the coast of Shandong province, China, *Chinese Science Bulletin, 53*(7):1079-1086.

Yang J., G. Lu, L. Lee, G. Feng, 2015, Long-delayed bright dancing sprite with large horizontal displacement from its parent flash, *J. Atmos. Sol. Terr. Phys., 129*, 1-5.

Yaniv, R., Y. Yair, C. Price, J. Bór, M. Sato, Y. Hobara, S. Cummer, J. Li, and A. Devir (2014), Ground-based observations of the relations between lightning charge-moment-change

and the physical and optical properties of column sprites, *J. Atmos. Sol. Terr. Phys., 107*, 60–67, doi:10.1016/j.jastp.2013.10.018.

Term	Signification	Typical order of duration
Period	Part of the storm lifetime during which several sprites are detected	hour
Event	Video including sprite elements	second
Sequence	Succession of video fields with sprite elements following a same stroke	tenth of second
Field	de-interlaced video frames	20 ms

Table 1. Terminology used for the sprite activity at several scales of time.

Sprite event					SP+CG stroke					
	Time (UTC)				Time (s)	Distance camera (km)	Peak current (kA)	Δt sprite (ms)	CMC (C km)	iCMC (C km)
hh:mm	t_1 (s)	t_2 (s)	dt (ms)	Frame						
18:03	8.891	9.091	200	F1-F10	8.829	465	57	62-82	8755	174
	9.531	9.751	220	F33-F43	9.528	432	34	3-23	1611	121
	10.111	10.311	200	F62-F71	10.123	400	79	0-8	5009	460
	10.511	10.631	120	F82-F87	10.516	367	152	0-15	6935	839
18 :08	20.094	20.194	100	F1-F5	20.054	420	26	40-60	-	-
	20.254	20.494	240	F9-F20	-	-	-	-		
	20.614	20.894	280	F27-F40	20.626	379	97	0-8	5277	440
	20.894	20.934	40	F41-F42	20.899	370	84	0-15	3831	543

Table 2. Characteristics of the two series of sprite sequences and SP+CG strokes associated. For the timing of the optical events: t_1, t_2 and dt are times of beginning and end, and duration of a sprite sequence with continuous luminosity, respectively. For each SP+CG stroke: time in second, distance to the camera, peak current, time delay Δt between the stroke and the beginning of the sprite sequence, CMC and impulsive CMC (iCMC).

Figure captions

Figure 1. a) Location of the -CG, +CG flashes and SP+CG strokes detected during the storm lifetime. The color indicates the time for every three hours. b) and c) CTT at 1110 and 1610 UTC, respectively. The CG flashes detected during 10 minutes around the time of the scan are plotted with white crosses and red pluses for –CG and +CG, respectively.

Figure 2: Time series of rates of the CG flash (white histogram for –CG, grey histogram for +CG), minimum value of the cloud top temperature T_m (solid line), and areas with CTT < -40°C A(-40) (dashed line) and A(-65) (line with dots). The scale for the areas is in 10^4 km^2 and A(-65) values are multiplied by 10. The periods indicated with arrows correspond to observation of sprite events between 1749 and 1841 UTC, between 2130 and 0239 UTC, and presence of cloud at the Pic du Midi site between 1841 and 2130 UTC.

Figure 3. CTT at the Meteosat scan times: 1810 UTC (a) and 1825 UTC (b). The CG flashes (strokes) detected during 10 minutes centered around the time of the scan are reported with white crosses and small (large) red pluses for -CG and +CG (SP+CG), respectively. Maximum radar reflectivity in the same area: (c) at 1810 UTC with SP+CG strokes (red crosses) between 1800 UTC and 1815 UTC and (d) at 1820 UTC with SP+CG strokes between 1815 UTC and 1830 UTC. The SP+CG strokes are indicated with red crosses. The colored scale in dBZ for the radar reflectivity is indicated below the graphs.

Figure 4: Case of the series of sprite sequences at 1803:08. (a) 8 specific fields issued from the video imagery numbered from F1 that is the first field with sprite luminosity. The altitude is in km. The white line indicates the line of sight of a sprite element (sometimes the brightest one, sometimes a central one) from the camera also reported in (b). (b) CTT at 1810 UTC with different symbols superimposed for the lines of sight reported in each field of (a), the -CG strokes (colored small cross), the +CG stroke (red plus), the SP+CG strokes (colored large plus) and the IC strokes (colored circles). (c) Peak current versus time for -CG strokes (blue cross), +CG strokes (red plus), SP+CG strokes (large and colored plus) and VHF sources detected by the XDDE (colored dots plotted with an arbitrary current value of 120 kA) versus time for 3

886 seconds. The red curve displays the current waveform on the secondary axis. (d) Electric field
887 radiated in VLF/LF range for the same period of 3 seconds (t = 0 corresponds to t = 9.528 s in
888 the graph of c)) at a resolution of 1 ms (upper graph) and 10 ms (lower graph).
889
890 Figure 5: As in Figure 4 for the series of sprite sequences at 1808:20. In (a) F2 is the second field
891 with sprite luminosity. In (d), t = 0 corresponds to t = 20.626 s in the graph of c)).
892
893 Figure 6. Maximum radar reflectivity with the lightning activity, SP+CG strokes (white crosses),
894 VHF sources (red dots), and -CG strokes (white dots) associated with both case studies of
895 dancing sprite: (a) at 1803 UTC and (b) at 1810 UTC. The colored scale in dBZ is indicated
896 below the graphs.
897
898 Figure 7. (a) and (b) Maximum radar reflectivity at two times of the cloud system at 1610 UTC
899 and 1710 UTC. The scale in dBZ is indicated in Figure 6. (c) and (d) CTT at the Meteosat scan
900 times at 1610 UTC and 1825 UTC. The CG flashes detected during 10 minutes centered around
901 the time of the scan are reported with white crosses and red pluses for -CG and +CG,
902 respectively.
903
904 Figure 8. a) Left: Current moment waveform (upper graph) and charge moment change (lower
905 graph) for a period of 600 ms during the dancing sprite event at 1803 UTC (t = 0 corresponds to
906 1803:8.829s). Right: four fields from the video imagery with sprite elements at times marked in
907 the graphs (one field is 20 ms). The altitude is in km. b) Same as a) for another period of 600 ms
908 (t = 0 corresponds to 1803:10.516s). The arrows in the fields show the caps (c and c') and the
909 bodies (b and b') for short (c and b) and long (c' and b') time-delayed sprite elements. The scale
910 altitude is determined according to the conditions explained in section 2.1.
911
912 Figure 9. Same as Figure 8 for a period of 500 ms during the dancing sprite event at 1808 UTC (t
913 = 0 corresponds to 1808:20.626s).
914
915 Figure 10. Electric field radiated in ELF/VLF/LF range (for upper/central/lower graphs) versus
916 time during 120 ms. a) case of the dancing sprite event at 1803 UTC (t = 5 ms corresponds to

1803:10.123). b) case of the dancing sprite event at 1808 UTC (t = 5 ms corresponds to 1808:20.899).

Figure 11. A detailed view of the current moment waveform for three cases of lightning strokes selected from Figures 4c and 5c: a) t = 0 corresponds to 1803:10.123 UTC, b) t = 0 corresponds to 1803:10.516 UTC, c) t = 0 corresponds to 1808:20.899 UTC.

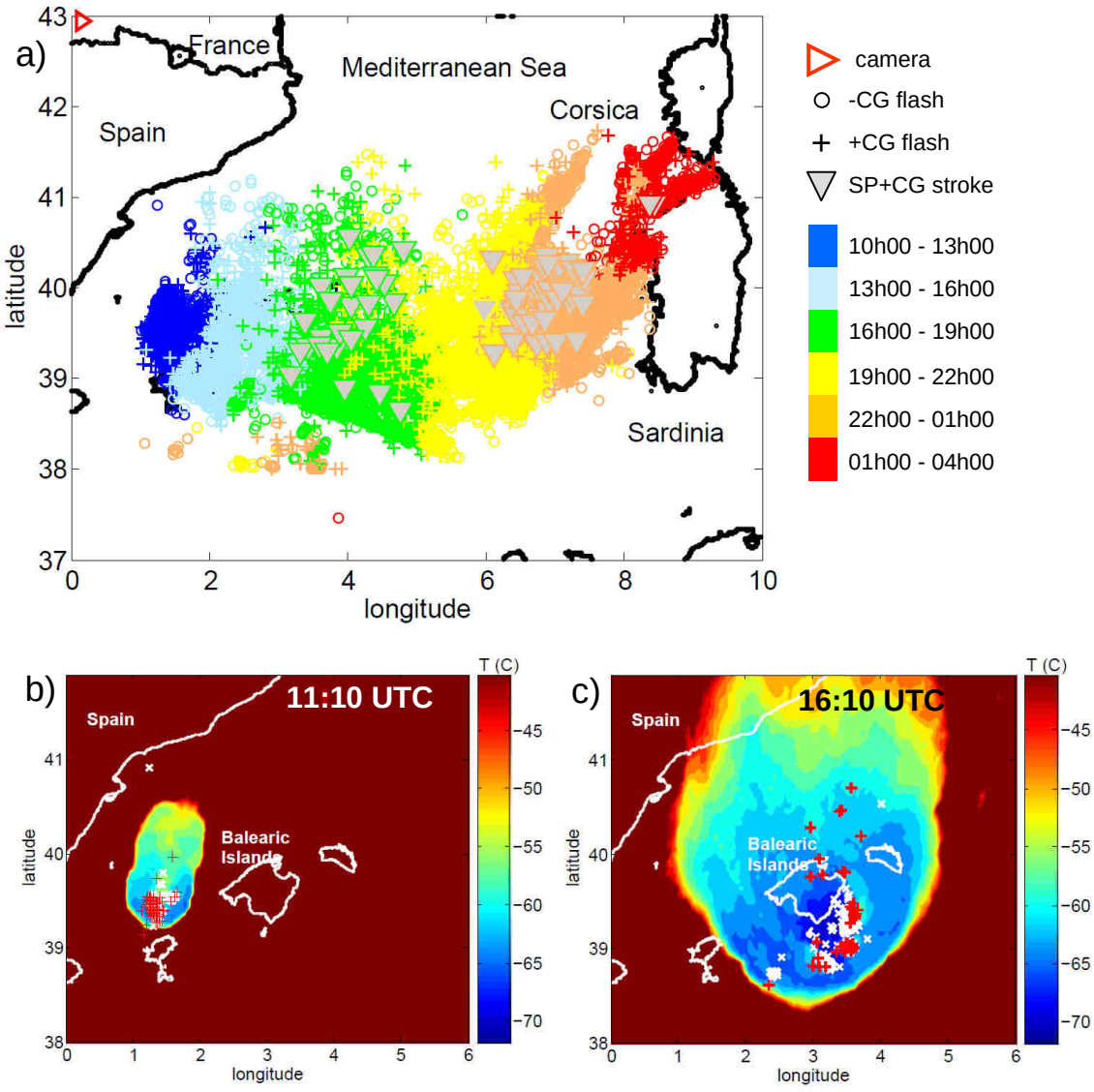

Figure 1: a) Location of the -CG, +CG flashes and SP+CG strokes detected during the storm lifetime. The color indicates the time for every three hours. b) and c) CTT at 1110 and 1610 UTC, respectively. The CG flashes detected during 10 minutes around the time of the scan are plotted with white crosses and red pluses for –CG and +CG, respectively.

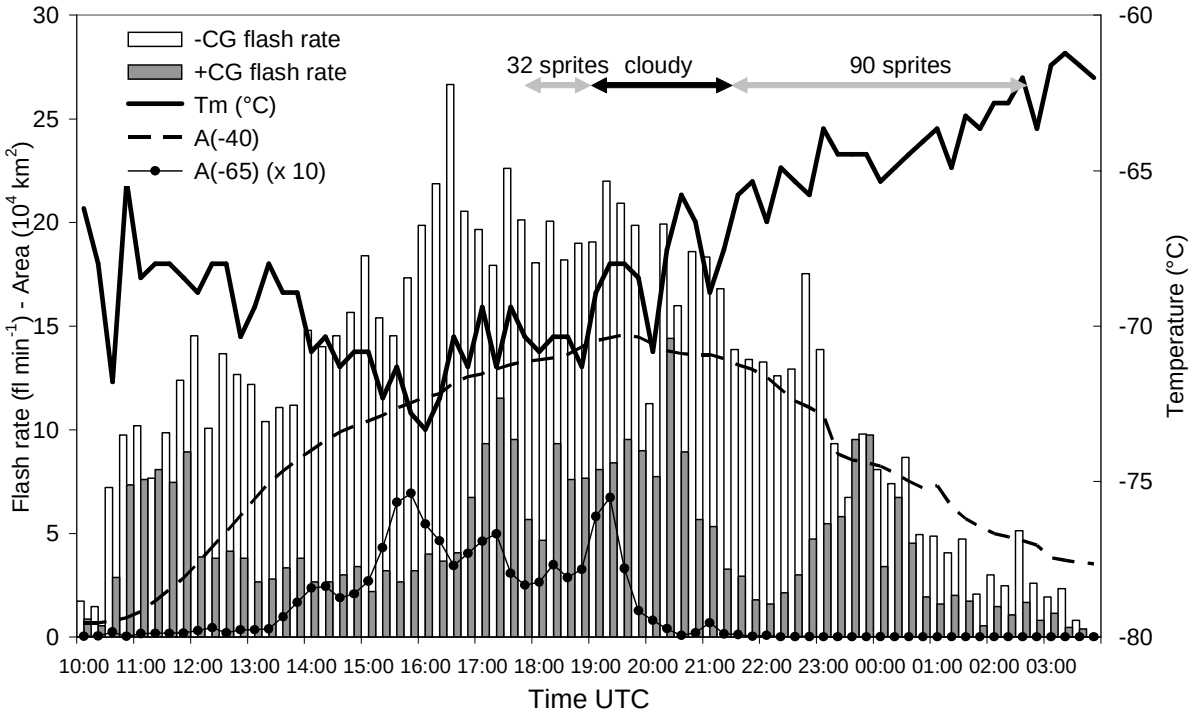

Figure 2: Time series of rates of the CG flash (white histogram for –CG, grey histogram for +CG), minimum value of the cloud top temperature T_m (solid line), and areas with CTT < -40°C A(-40) (dashed line) and A(-65) (line with dots). The scale for the areas is in 10^4 km^2 and A(-65) values are multiplied by 10. The periods indicated with arrows correspond to observation of sprite events between 1749 and 1841 UTC, between 2130 and 0239 UTC, and presence of cloud at the Pic du Midi site between 1841 and 2130 UTC.

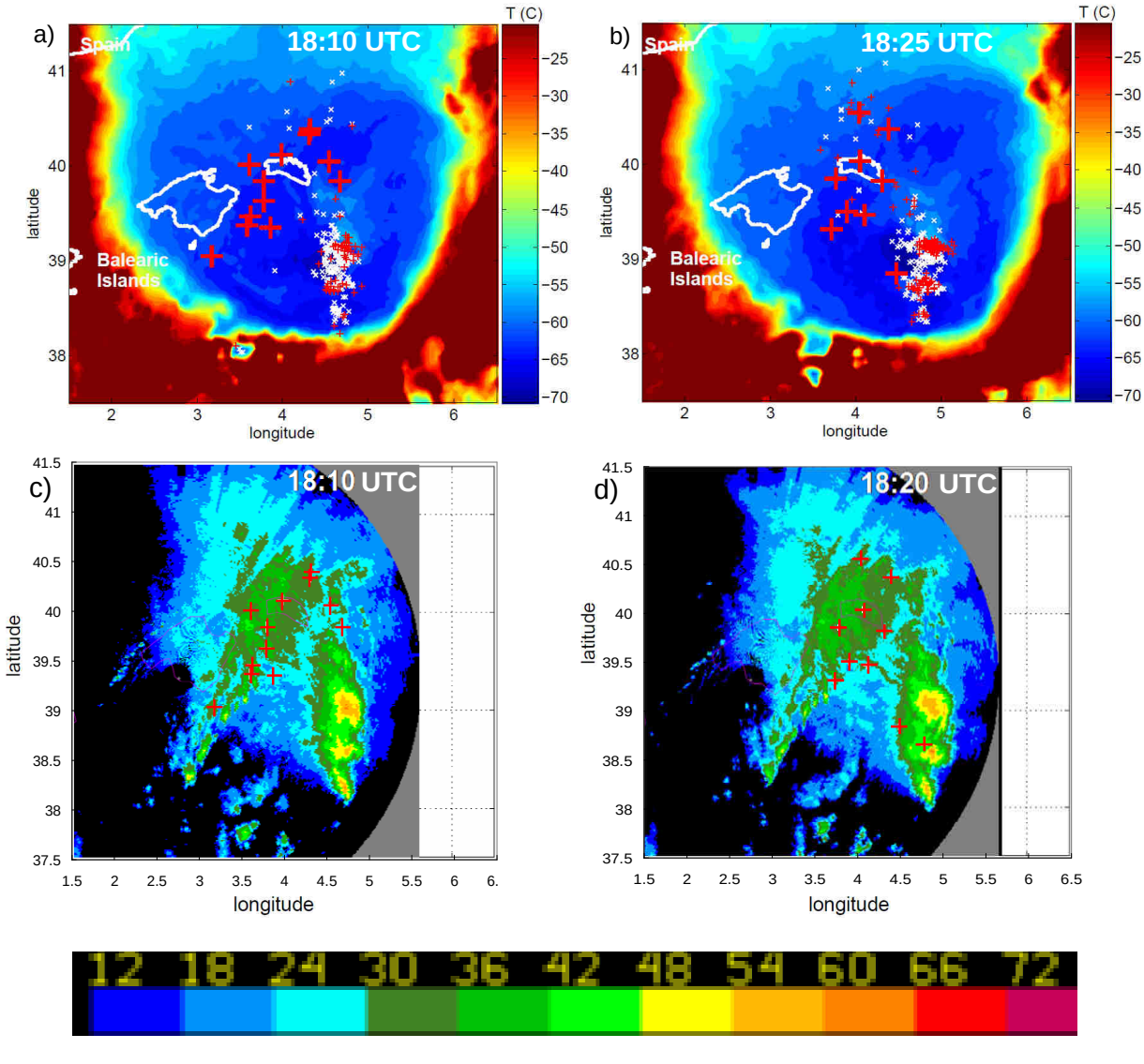

Figure 3. CTT at the Meteosat scan times: 1810 UTC (a) and 1825 UTC (b). The CG flashes (strokes) detected during 10 minutes centered around the time of the scan are reported with white crosses and small (large) red pluses for -CG and +CG (SP+CG), respectively. Maximum radar reflectivity in the same area: (c) at 1810 UTC with SP+CG strokes (red crosses) between 1800 UTC and 1815 UTC and (d) at 1820 UTC with SP+CG strokes between 1815 UTC and 1830 UTC. The SP+CG strokes are indicated with red crosses. The colored scale in dBZ for the radar reflectivity is indicated below the graphs.

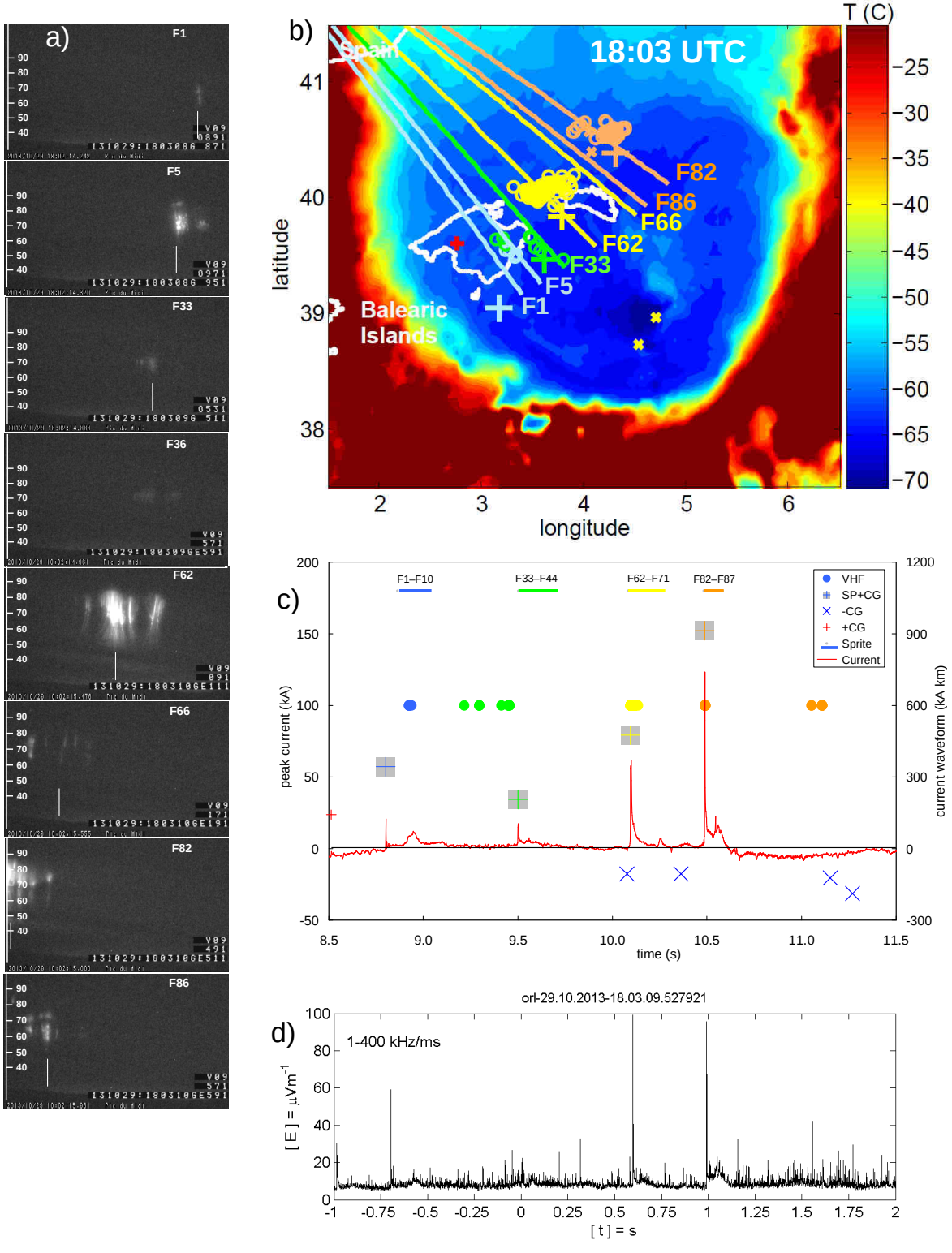
a)
F1
F5
F33
F36
F62
F66
F82
F86
b)
18:03 UTC
Spain
Balearic Islands
F82
F86
F66
F62
F33
F5
F1
T (C)
latitude
longitude
c)
F1–F10
F33–F44
F62–F71
F82–F87
VHF
SP+CG
-CG
+CG
Sprite
Current
peak current (kA)
current waveform (kA km)
time (s)
d)
orl-29.10.2013-18.03.09.527921
1-400 kHz/ms
[E] = µVm-1
[t] = s

Figure 4: Case of the series of sprite sequences at 1803:08. (a) 8 specific fields issued from the video imagery numbered from F1 that is the first field with sprite luminosity. The altitude is in km. The white line indicates the line of sight from the camera reported in (b). (b) cloud top temperature at 1810 UTC with different symbols superimposed for the lines of sight reported in each field of (a), the -CG strokes (colored small cross), the +CG stroke (red plus), the SP+CG strokes (colored large plus) and the IC strokes (colored circles). (c) peak current versus time for -CG strokes (blue cross), +CG strokes (red plus), SP+CG strokes (large and colored plus) and VHF sources detected by the XDDE (colored dots plotted with an arbitrary current value of 120 kA) versus time for 3 seconds. The red curve displays the current waveform on the secondary axis. (d) Electric field radiated in VLF/LF range for the same period of 3 seconds at a resolution of 1 ms (t = 0 corresponds to t = 9.528 s in c).

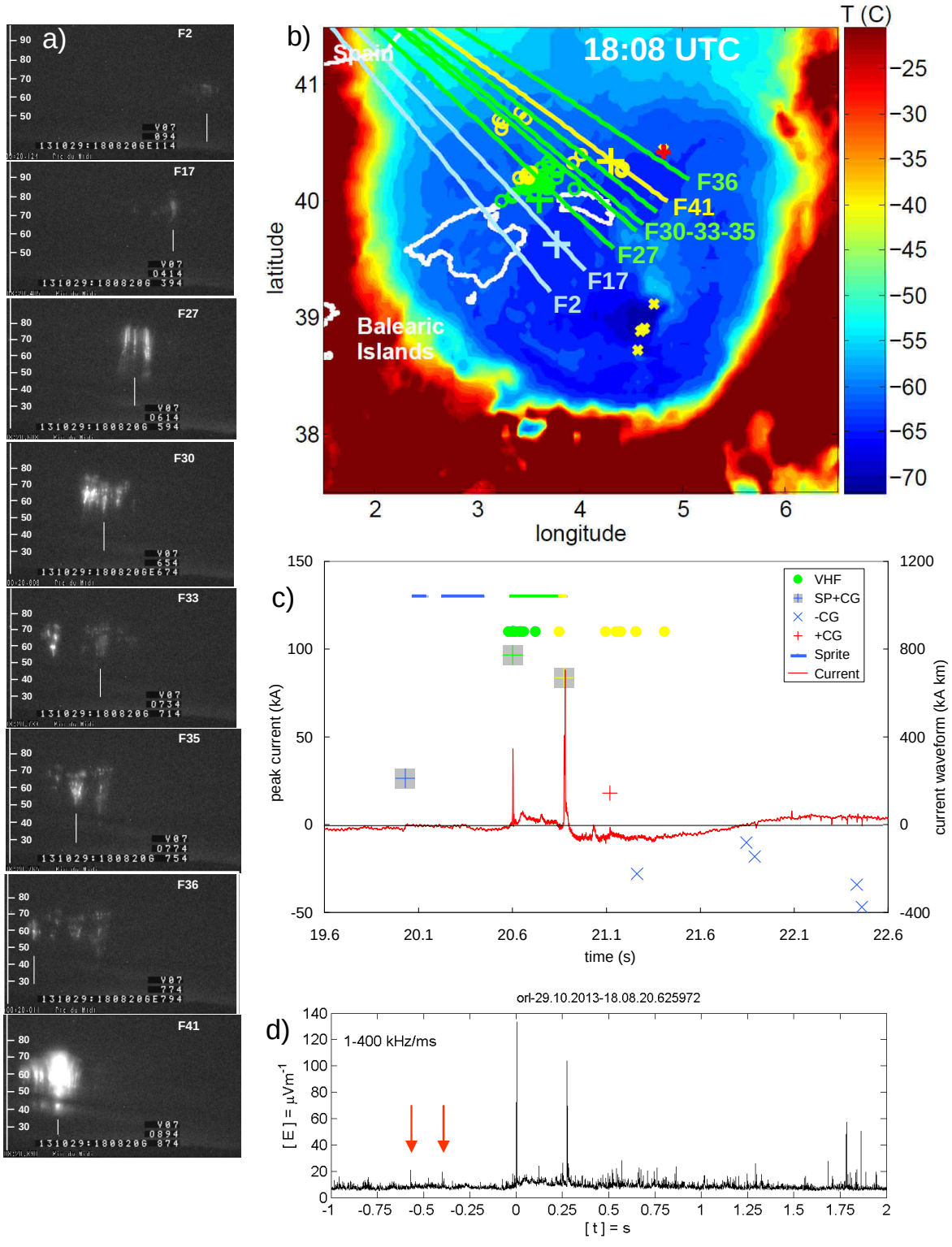
a)
F2
F17
F27
F30
F33
F35
F36
F41
b)
18:08 UTC
Spain
Balearic Islands
F36
F41
F30-33-35
F27
F17
F2
latitude
longitude
T (C)
c)
VHF
SP+CG
-CG
+CG
Sprite
Current
peak current (kA)
current waveform (kA km)
time (s)
d)
orl-29.10.2013-18.08.20.625972
1-400 kHz/ms
[E] = µVm-1
[t] = s

Figure 5: As in Figure 4 for the sprite event at 1808:20. In (a) F2 is the second frame with sprite luminosity. In (d), t = 0 ms corresponds to t = 20.626 s in c).

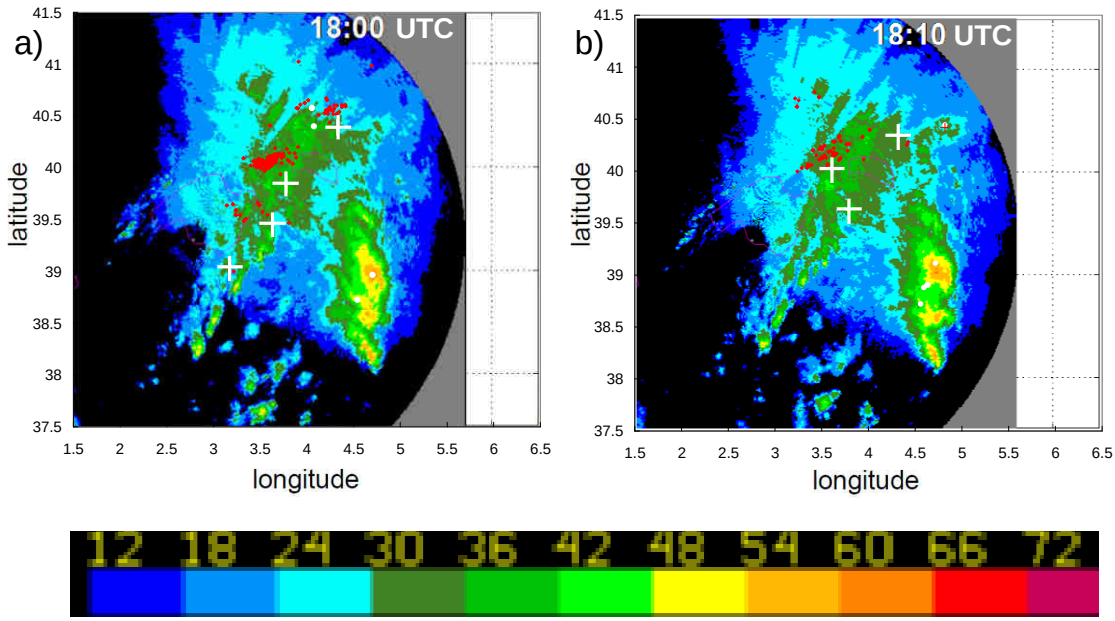

Figure 6. Maximum radar reflectivity with the lightning activity, SP+CG strokes (white crosses), VHF sources (red dots), and -CG strokes (white dots) associated with both case studies of dancing sprite: (a) at 1803 UTC and (b) at 1810 UTC. The colored scale in dBZ is indicated below the graphs.

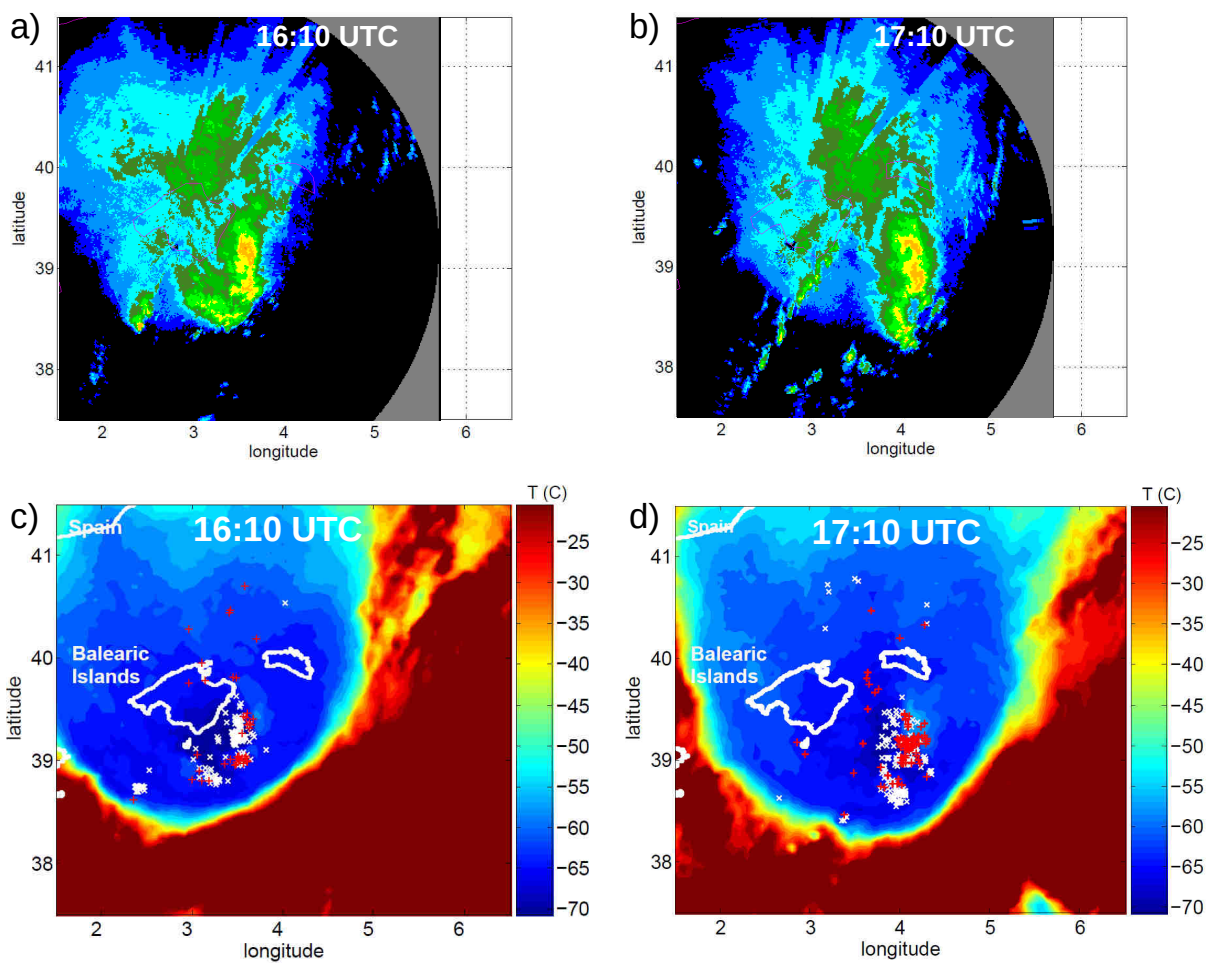

Figure 7. (a) and (b) Maximum radar reflectivity at two times of the cloud system at 1610 UTC and 1710 UTC. The scale in dBZ is indicated in Figure 6. (c) and (d) CTT at the Meteosat scan times at 1610 UTC and 1825 UTC. The CG flashes detected during 10 minutes centered around the time of the scan are reported with white crosses and red pluses for -CG and +CG, respectively.

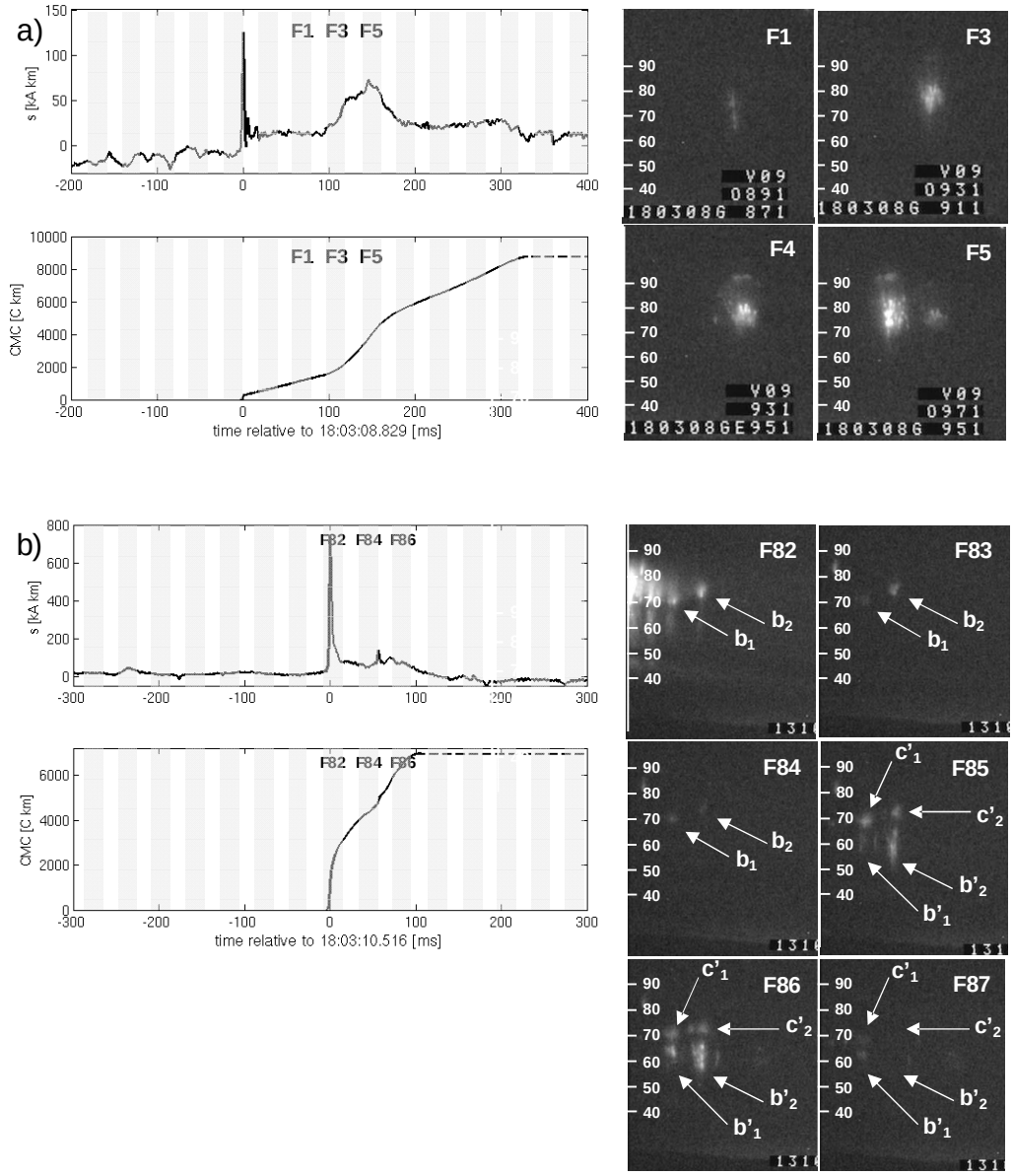

Figure 8. a) Left: Current moment waveform (upper graph) and charge moment change (lower graph) for a period of 600 ms during the dancing sprite at 1803 UTC (t = 0 corresponds to 1803:8.829s). Right: four fields from the video imagery with sprite elements at times marked in the graphs (one field is 20 ms). The altitude is in km. b) Same as a) for another period of 600 ms (t = 0 corresponds to 1803:10.516s). The arrows in the fields show the caps (c and c') and the bodies (b and b') for short (c and b) and long (c' and b') time-delayed sprite elements.

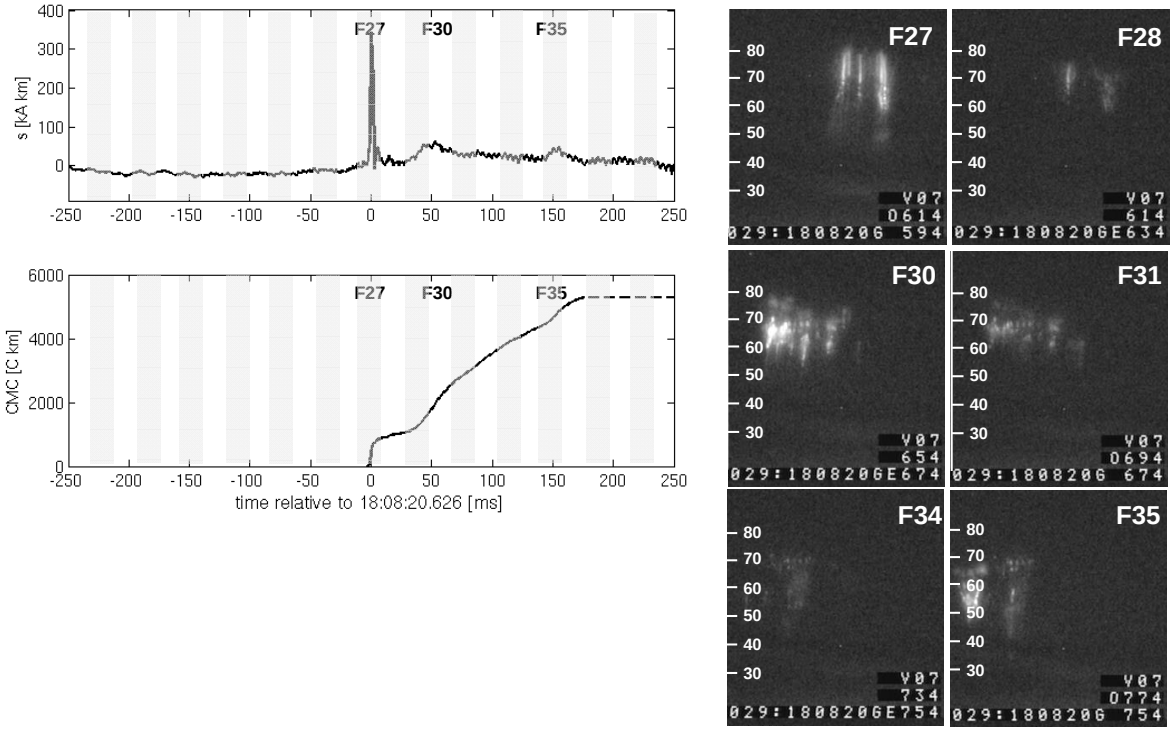

Figure 9. Same as Figure 8 for a period of 500 ms during the dancing sprite event at 1808 UTC (t = 0 corresponds to 1808:20.626s).

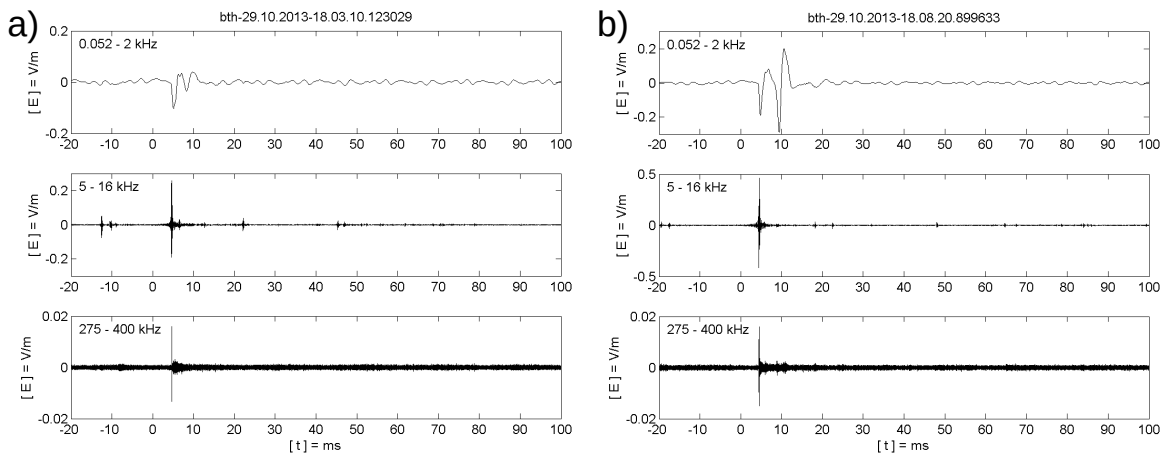

Figure 10. Electric field radiated in ELF/VLF/LF range (for upper/central/lower graphs) versus time during 120 ms. a) case of the sprite event at 1803 UTC (t = 5 ms corresponds to 1803:10.123). b) case of the sprite event at 1808 UTC (t = 5 ms corresponds to 1808:20.899).

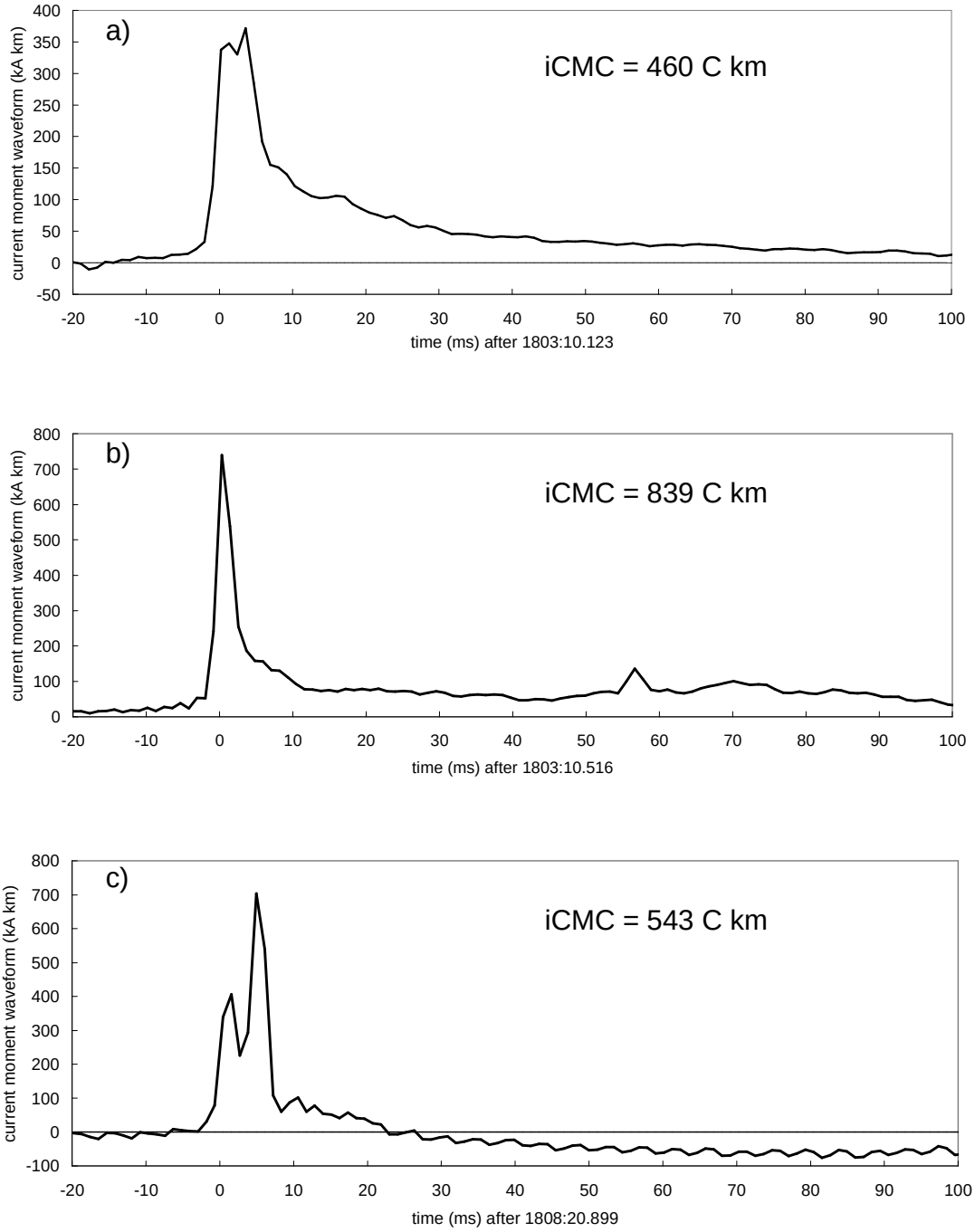

Figure 11. A detailed view of the current moment waveform for three cases of lightning strokes selected from Figures 4c and 5c: a) t = 0 corresponds to 1803:10.123 UTC, b) t = 0 corresponds to 1803:10.516 UTC, c) t = 0 corresponds to 1808:20.899 UTC.